

Influence of South America orography on summertime precipitation in Southeastern South America

C. Junquas^{1,2} · L. Li³ · C. S. Vera⁴ · H. Le Treut³ · K. Takahashi¹

Received: 7 August 2014 / Accepted: 24 August 2015 / Published online: 5 September 2015
© Springer-Verlag Berlin Heidelberg 2015

Abstract Impacts of the main South American orographic structures (the Andes, the Brazilian Plateau and the Guiana shield) on the regional climate and associated global teleconnection are investigated through numerical experiments in which some of these features are suppressed. Simulations are performed with a “two-way nesting” system coupling interactively the regional and global versions of the LMDZ4 atmospheric general circulation model. At regional scale, the simulations confirm previous studies, showing that both the Andes and the Brazilian Plateau exert a control on the position and strength of the South Atlantic convergence zone (SACZ), mainly through their impact on the low-level jet and the coastal branch of the subtropical anticyclones. The northern topography of South America appears to be crucial to determine the leading mode of rainfall variability in eastern South America, which manifests itself as a dipole-like pattern between Southeastern South America and the SACZ region. The suppression of South America orography also shows global-scale effects, corresponding to an adjustment of the global circulation system. Changes in atmospheric circulation and precipitation are found in remote areas on the globe, being the consequences of various teleconnection mechanisms. When the Brazilian

Plateau and the Andes are suppressed, there is a decrease of precipitation in the SACZ region, associated with a weakening of the large-scale ascendance. Changes are described in terms of anomalies in the Walker circulation, meridional displacements of the mid-latitude jet stream, Southern annular mode anomalies and modifications of Rossby wave train teleconnection processes.

Keywords South America orography · Summer precipitation · Orography influence · Two-way nesting system · Global teleconnection processes

1 Introduction

The South America topography is composed of different structures, the most important being the Andes in the western flank, the Guiana shield in the north and the Brazilian Plateau (BP) in the east. They exert individually distinct influences on the regional climate.

The influence of the Andes over the atmospheric circulation features has been assessed in previous studies, but is still subject to large uncertainties. Using global and regional climate models, some of these studies tend to show that the Andes have little control over the large-scale circulation components of the South America monsoon system, like the Bolivian High and the Northeastern Low, since these structures are mainly atmospheric responses to diabatic heating released by the summer precipitation over the Amazon basin (e.g., Figueroa et al. 1995; Rodwell and Hoskins 2001). However, other studies using regional climate models indicate that the presence of the Andes does exert an influence on the continental-scale atmospheric circulation gyre observed at low levels with large impact on moisture transport (e.g., Gandu and Geisler 1991; Insel et al. 2010;

✉ C. Junquas
clementine.junquas@gmail.com

¹ Instituto Geofísico del Perú (IGP), Lima, Peru

² IRD/UJF-Grenoble 1/CNRS/G-INP, LTRE UMR, 5564 Grenoble, France

³ Laboratoire de Météorologie Dynamique, Institut Pierre Simon Laplace, UPMC/CNRS, Paris, France

⁴ Centro de Investigaciones del Mar y la Atmosfera (CIMA/CONICET-UBA), DCAO/FCEN, UMI IFAECI/CNRS, Buenos Aires, Argentina

Saurral et al. 2014). In particular, the South American low-level jet (LLJ) centered over Bolivia, is thought to be, to a large extent, mechanically forced by the Andes all-year around (e.g., Campetella and Vera 2002). The LLJ is a key element of moisture transport from the tropical to subtropical regions of South America (e.g., Berbery and Barros 2002). During summer, the thermodynamic forcing associated with tropical convection and the mechanical forcing induced by the Andes combine together to determine the dynamics of the LLJ. The subtropical plains situated in Southeastern South America (SESA) includes La Plata basin, and covers northern Argentina, Uruguay and southern Brazil. In SESA, an area with very dense population, agriculture and hydroelectric power generation are severely affected by the summertime variability of precipitation, which is in turn largely influenced by the LLJ variability. Partly due to the successful SALLJEX experiment, considerable progress has been made in understanding the LLJ dynamics and its influences on tropical and subtropical precipitation variability (e.g., Vera et al. 2006). However the combined influence of the South American Monsoon System and South American topography, in explaining the main features of the continental-scale moisture transport and associated precipitation has rarely been explored. The main goal of this study is to identify the relative role of the different elements of South America topography in explaining climate features over South America, particularly over the continental portion located to the east of the Andes.

The orographic influence of the BP on South American precipitation characteristics has also been explored in the literature, and particular attention was paid to the South Atlantic Convergence Zone (SACZ), a rainfall band extending from the Amazon basin toward Southeastern Brazil (e.g., Kodama 1992). By statistically analyzing 27 years of austral summer reanalysis data, Kodama et al. (2012) found that there are enhanced rainfalls when the SACZ coastal portion develops right over the BP maximum topography in Southeastern Brazil. Grimm et al. (2007) and Kodama et al. (2012) used limited-domain climate models with a 60- and 25-km horizontal resolution respectively, to perform case studies and sensitivity tests in South America with different BP topography forcing. Their results suggest that BP plays an important role in anchoring the SACZ at its actual climatological position. Precipitation variability in the SACZ region is closely linked to that in SESA at a large range of timescales, from intraseasonal (e.g., Nogués-Paegle and Mo 1997), interannual (e.g., Doyle and Barros 2002) to much longer time scales (e.g., Robertson and Mechoso 2000). Precipitation variability in the SACZ and SESA regions is highly related and characterized by a dipole with centers of action of opposite sign located in the two regions respectively. Precipitation in SESA is then largely affected by the position and intensity of the SACZ. Grimm et al.

(2007) pointed out that BP plays a crucial role in creating and maintaining the dipole-like precipitation mode. In their simulation with BP excluded, an anticyclonic circulation anomaly is obtained between La Plata basin and southeastern Brazil, which shifts the SACZ toward the southwest, and increases the precipitation in SESA. However, as the Andes play a role in transporting moisture further south, it is not clear yet how the combined influence of both Andes and BP topographies contributes to determine the main climatic features at both SACZ and SESA regions. Although these studies brought an increased understanding of the role of South America orography on regional climate, a majority of them may be affected by limitations in terms of limited domain and coarse spatial resolution. This concern is also enhanced because South-America is an area where regional and global changes are strongly interacting.

As noted above, there are evidences indicating that the Andes not only affect the South American regional climate, but also exert influence remotely on the Inter-tropical convergence zone (ITCZ) and South Pacific convergence zone (SPCZ). Takahashi and Battisti (2007a, b) showed that the presence of the Andes is crucial for models to simulate cold SST off the west coast of South America. Xu et al. (2004) showed that their presence induces a strengthening of the dry and cool region in the southeastern Pacific Ocean, off the coast of western South America. By blocking the warm westward flow from the Amazon region, the Andes help to maintain the cloud-radiation feedback west of the Andes, a dry zone characterized by low-level stratocumulus clouds trapped in a strong temperature inversion (e.g., Bretherton 1993; Wyant et al. 1997; Yuter et al. 2000; Garreaud et al. 2001). Feedbacks in this region regulate strongly the global climate sensitivity. Rodwell and Hoskins (2001) showed that the presence of the Andes is associated with a zone of dry subsidence in the West, corresponding to the eastern branch of the South Pacific Anticyclone (SPA). This subsidence contributes to reduce SST west of the Andes through evaporation mechanisms (Takahashi and Battisti 2007a). Moreover, the northwestward circulation related to the northern SPA is associated with a low-level advection of moist static energy by the trade winds contributing to the expansion of the dry zone westward along the equator. These processes mainly explain the North–South Pacific asymmetry, with the ITCZ present only in the northern hemisphere most of the year (Mitchell and Wallace 1992). On the other hand, Takahashi and Battisti (2007b) showed that through the northwestward propagation of the dry zone and the SPA, the Andes are also related to the position and shape of the SPCZ. They argued that the presence of the Andes influences the width of the subtropical part of the SPCZ by controlling the separation between its tip and the coast of South America. In return, via Rossby wave train development and teleconnection processes, the variability

of such Pacific features like the double-ITCZ and the SPCZ can influence circulation anomalies in South America, and in particular alter precipitation anomalies in the SESA region (Karoly 1989; Mo 2000; Silva et al. 2009; Grimm et al. 2000). However, it has not been thoroughly studied yet how much of the South America topography can affect the large-scale teleconnection processes.

This is why, in this paper, we want to revisit the issue of orographic impacts on the South American climate, using a comprehensive global climate model. In addition, as mentioned before, previous studies have already performed independently sensitivity orography test of the BP (Kodama et al. 2012; Grimm et al. 2007), or the Andes (e.g., Figueroa et al. 1995; Insel et al. 2010; Saurral et al. 2014). However, in this study we perform for the first time, to our knowledge, both BP and Andes sensitivity experiments with the same model configuration. Therefore a first specific objective of the work is to assess the respective role of the Andes and BP, and their combined effects, on the main structures of precipitation and atmospheric circulation in South America during the austral summer. Another objective of our work is to gain further insight in the physical processes that determine this influence.

We therefore need to study the influence of the South America topography on both regional and global climate features, and the interaction between the two. For this purpose, we use in this paper a numerical climate platform allowing for “two-way nesting” (TWN). The TWN system consists in the two-way interaction between a regional and a global climate model, specifically designed for studies of regional-global-regional scale interaction processes (Lorenz and Jacob 2005; Chen et al. 2011; Junquas et al. 2013).

The paper is organized as follows. In Sect. 2 the data, model and performed experiments are described. In Sect. 3 we analyze the regional influence of the Andes and the BP orography over South America, with particular focus over the eastern part of the continent and the SESA/SACZ dipole-like region. The global atmospheric circulation changes induced by both orography structures are then studied in Sect. 4. Finally, results are summarized and discussed in Sect. 5.

2 Model, experiments and data

2.1 Description and validation of the model

This study uses the same TWN system as in Junquas et al. (2013), based on a regional and a global version of the LMDZ4 model (Li 1999; Hourdin et al. 2006), and called “TWN-LMDZ”. The LMDZ4 model is the atmospheric component of the Institut Pierre Simon Laplace Coupled Model (IPSL-CM4; Marti et al. 2005). This TWN

system was largely described in Junquas et al. (2013). The TWN technique consists of running in parallel a regional model and a global model (Lorenz and Jacob 2005). In this case, the global model is the “LMDZ-global” with a regular horizontal grid of 96×72 points, and a resolution of $2.5^\circ \times 3.75^\circ$. The regional model is the “LMDZ-regional” with a global grid of 120×121 points, stretched over South America, where the regional horizontal resolution is about 100 km. The two model configurations share the same physical parameterizations and the same vertical discretization (19 hybrid levels), and only differ in their horizontal spatial resolutions. Through the TWN technique, interactions between the regional and global models allow an improvement of teleconnection processes from global to regional climate, and of feedbacks from regional to global climate. Junquas et al. (2013) showed that using LMDZ4 with the TWN technique improves the representation of the precipitation over South America, as well as its associated global atmospheric circulation. Observed SST and sea ice component (SIC) distribution data from the Atmospheric Model Intercomparison Project AMIP (Gates 1992) are used as boundary conditions for both LMDZ-regional and LMDZ-global, and for each experiment.

In this paper, the influence of the Andes and the BP topography will be explored at a regional and global scale. With a 100-km resolution, the model is able to simulate the main regional climate characteristics associated with the SESA climate as well as the SACZ or the LLJ (Junquas et al. 2013). However, localized climate features are not analyzed here and would need a dynamical downscaling for finer resolution. Junquas et al. (2013) already assessed the main features of the precipitation field simulated by the model (their Fig. 4), and identified some structures which are well represented when compared to CMAP data (Xie and Arkin 1997): the Atlantic ITCZ, the maximum related with the South America monsoon system in central Brazil, the Northwest-Southeast oriented band defining the SACZ, and a minimum in the northeast of Brazil.

Junquas et al. (2013) also identified some biases associated with orography: overestimations over the central and northern Andes, and over the part of the SACZ situated over the BP maximum topography. Recently, the Tropical Rainfall Measurement Mission (TRMM; Kummerow et al. 2000; Huffman et al. 2007) provided a global climatological precipitation dataset at relatively high horizontal resolution (about 30 km). By comparing the model (Fig. 1c) to TRMM data (Fig. 1d), the previous remarks are still valid, and the higher resolution of TRMM shows additional features. In central and northern Andes, the zone of maximum precipitation is situated at the maximum altitude, while in TRMM it is situated in the eastern slope (cf. topography in Figs. 1a, b). In southeastern Brazil, the maximum precipitation associated with the coastal SACZ maximum is more

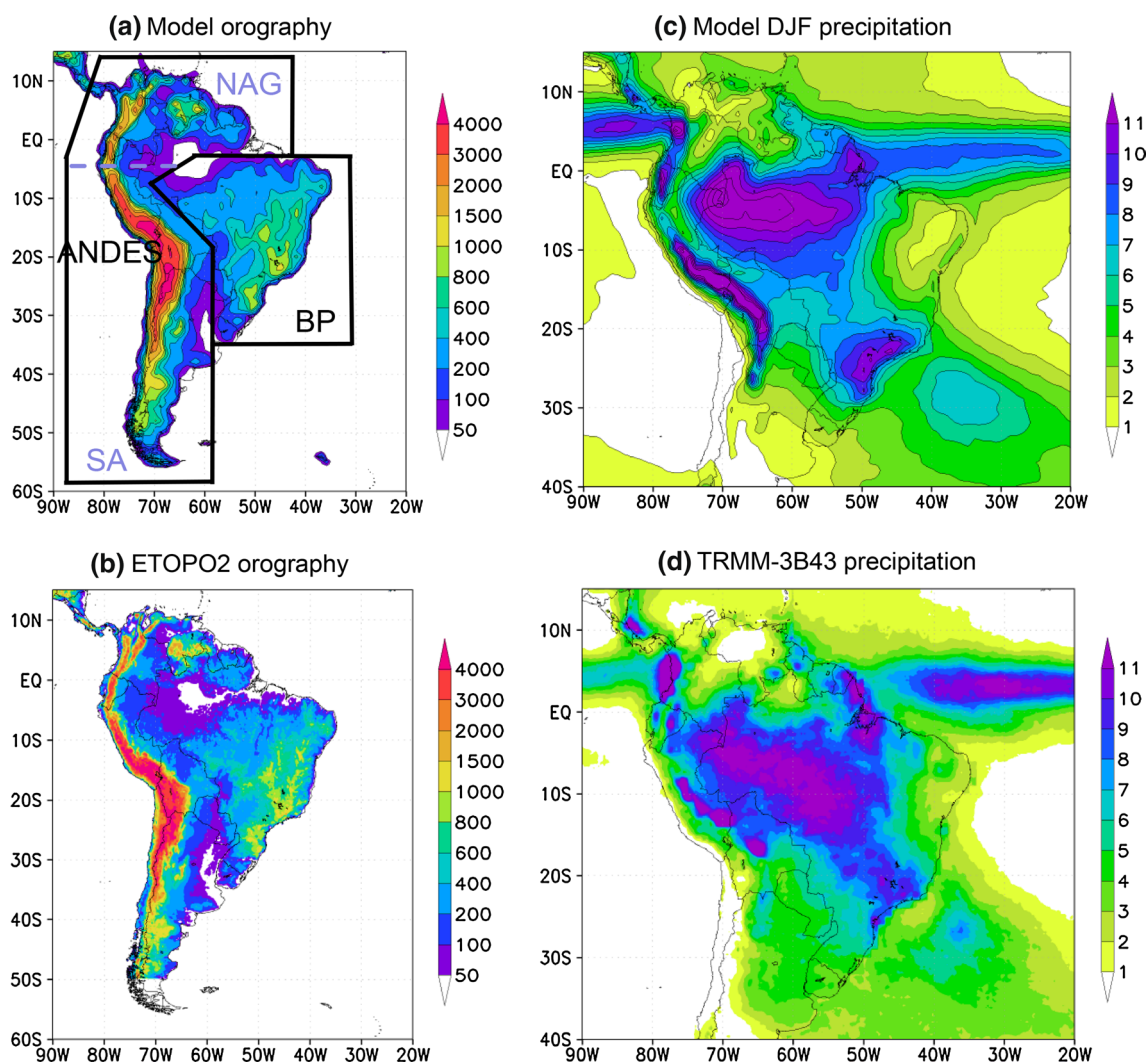


Fig. 1 Regional topography in m from **a** LMDZ-regional of CTRL, **b** ETOPO2, and DJF mean of precipitation in mm/day from **c** LMDZ-regional of CTRL, **d** TRMM 3B43 product

southwestward expanded than in TRMM data. In addition, while other precipitation data like CMAP and GPCP (Huffman et al. 2011) did not describe any maximum of precipitation in southeastern Brasil (Junquas et al. 2013), it is apparent in TRMM data (Fig. 1d) and some other observation datasets (e.g., Rozante et al. 2010, Carvalho et al. 2012), but less pronounced and less spatially extended than in the model (Fig. 1c).

Such a coastal SACZ maximum had already been identified by Codron and Sadourny (2002), using a previous version of LMDZ, and had been associated with an overestimated orographic precipitation. This bias basically consisted of a too strong moisture advection toward the summits and plateau with colder temperatures. Codron and Sadourny (2002) improved the water vapor advection scheme with a redistribution of moisture along the path, reducing the orographic bias by 20 % over the BP.

The bias is still persisting in LMDZ4, but to a less extent. Other studies have shown that using more elaborated vertical coordinates can also reduce the orographic precipitation bias (Simmons and Burridge 1981; Zhu 1997). When the pressure gradient error is reduced, the distribution of rainfall is more realistic in orographic regions, due to a better representation of the moisture advection and convergence. For instance, the Eta model (Mesinger et al. 1988), using *eta* vertical coordinates, reproduces realistic precipitation patterns over the Andes (Pesquero et al. 2010), with maximum precipitation in the foothills regions, and drier summits. However, the model still simulates an orographic precipitation maximum over the BP stronger than in the observations, although less pronounced than in LMDZ. In this paper, we will therefore need to evaluate how much the precipitation maximum simulated by the TWN-LMDZ control simulation is explained by the BP topography.

Table 1 List of experiments and their associated orography components

Run name	Topography related figure	Orography structures included		
		Brazilian plateau (BP)	ANDES	
			Southern Andes (SA)	Northern Andes and Guiana shield (NAG)
CTRL	Figure 1a	X	X	X
NOBP	Figure 2a		X	X
NOANDES	Figure 2b	X		
NOSA	Figure 8a	X		X

The CTRL experiment is indicated in bold

Junquas et al. (2013) also noted overestimated precipitations over the monsoon maximum in central Brazil, and underestimated precipitations in northeastern Brazil and over the subtropics. The cumulus parameterization in the model is represented by the Emanuel's scheme (e.g., Emanuel 1991). Previous papers have shown that this scheme provides a realistic spatial distribution of the convective precipitation (e.g. Hourdin et al. 2006; Braconnot et al. 2007; Davis et al. 2009). However, an over-estimation of the convective precipitation is generally found in tropical regions, in association with the use of this cumulus parameterization scheme. At global scale, the main model bias is associated with the representation of the convection over the maritime continent split in two separated regions, while observations show one contiguous rainfall region (Junquas et al. 2013). Overestimations of the tropical precipitation are also found in the western Indian Ocean and western SPCZ. The model does not display a Pacific double-ITCZ bias (see Introduction). However the SPCZ is simulated somewhat detached from the Indian-western Pacific Oceans equatorial band. It is not clear how these biases could affect the teleconnection processes. The strong Amazon convection could induce an overestimation of the mechanisms associated with the monsoon latent heat release. However, the model reproduces coherent large-scale circulation and teleconnections, including a realistic Amazon ascendance center when compared to the reanalysis data (Junquas et al. 2013).

2.2 Experiments

Experiments are listed in Table 1. The control simulation (named "CTRL") is the same as described in Junquas et al. (2013) and is used as a representative austral summer season (December–January–February, DJF). An ensemble of 30 DJF was simulated for each experiment by a random sampling of the atmospheric and land surface initial conditions (see Junquas et al. 2013 for more details on the methodology). The topography of South America used in CTRL is displayed in Fig. 1c. Related sensitivity experiments were characterized by the removal of different orographic structures, the surface height being then reduced to an upper limit of 50 m. The different modified orographic

configurations are (cf. Table 1 and Fig. 1a): (i) NOBP, with the BP topography removed, (ii) NOANDES with the Andes and the Guiana shield removed, and (iii) NOSA, where only the Andes to the south of 4°S were removed. As seen in Fig. 1c, we defined the BP domain as all the orography extending between the Amazon plain North of Brazil and the subtropical plains North of Argentina. The limits between the Andes and the BP, and between the northern and southern Andes are located in minimum topographic points. At each grid point where the orography is modified, new corresponding values of surface temperature and surface pressure are computed and introduced in the initial state. We also inhibit the parameterization of subgrid-scale orographic features for these points. The orography was gradually reduced, each step deleting only 100 m, with a 3-day simulation at each step to let the system to adapt progressively to the new topographic conditions. Each 100-m simulation step was forced by limit conditions corresponding to the three last days of October. Experiments begin in November with all selected grid points displaying topography of 50 m, and as explained in Junquas et al. (2013), this month is considered as a "spin-up", to let the system the time to absorb these initial perturbations.

The Andes orography as defined in this paper also includes the Guiana Shield (see Table 1). In order to explore how much the precipitation and its associated regional atmospheric circulation are controlled by both the northern Andes (including the Guiana shield), and the central and southern Andes, the NOSA (no-Southern Andes) experiment is performed. The results of this experiment are analyzed and compared with the results of the NOANDES experiment in the end of Sect. 3.2.

2.3 Data

The 3B43 product of the Tropical Rainfall Measuring Mission (TRMM) is used to analyze the climatological DJF precipitation (1998–2012) in Figs. 1d and 5a. TRMM-3B43 is a monthly compiled version of TRMM-3B42 which is a global multi-satellite precipitation analysis data set with a 0.25° horizontal resolution, and available between 50°S

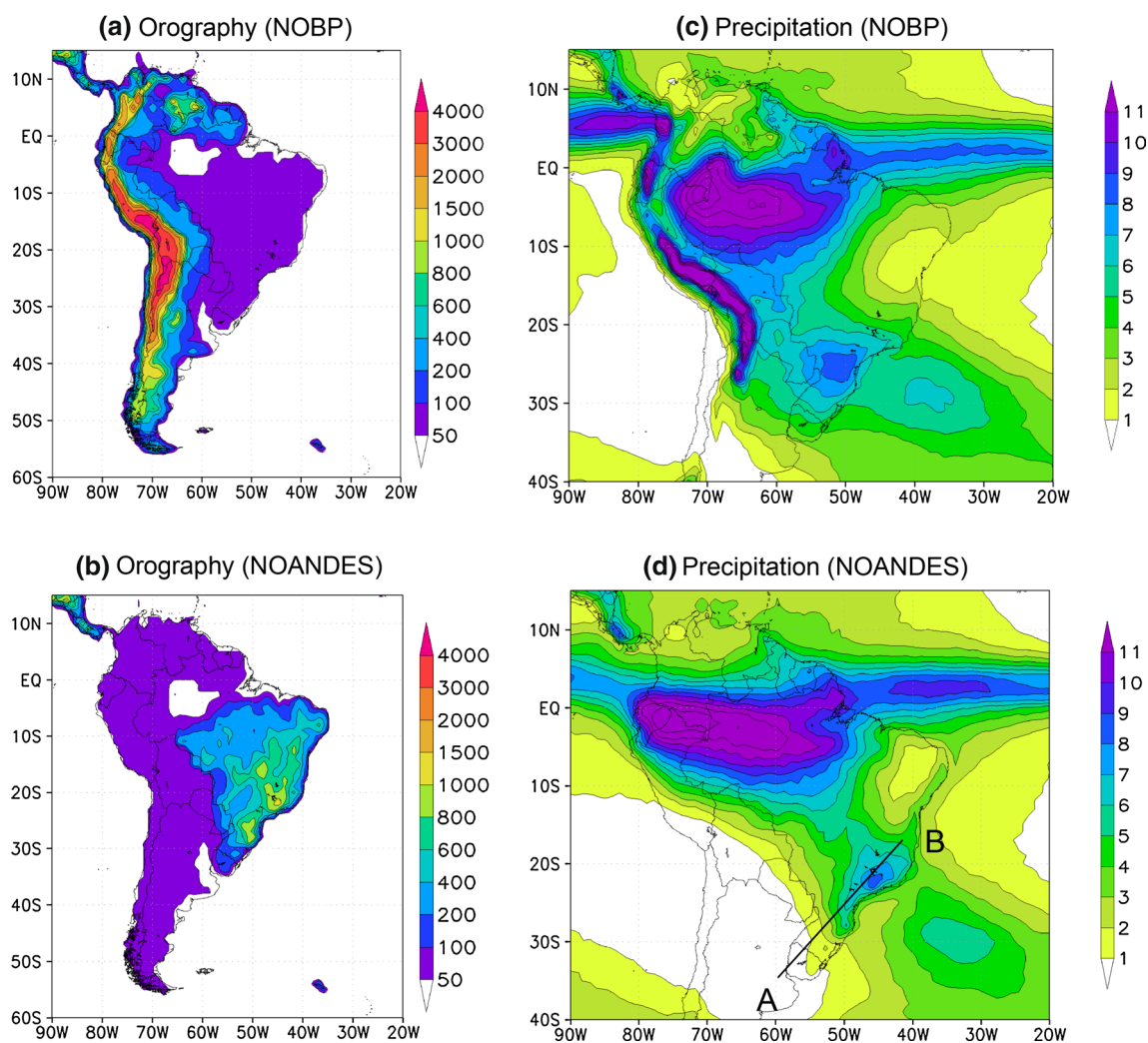


Fig. 2 Regional topography of LMDZ-regional of the **a** NOBP, and **b** NOANDES experiments in m, and DJF precipitation mean of the **c** NOBP, and **d** NOANDES experiments in mm/day

and 50°N latitude (Kummerow et al. 2000; Huffman et al. 2007). The topography data displayed in Fig. 1b is from the 2-min gridded global relief data ETOPO2v2 (NOAA NGDG 2001). The 20-DJF mean (1979–1999) of the reanalysis dataset NCEP/NCAR (Kalnay et al. 1996) from the NOAA/OAR/ESRL PSD, Boulder, Colorado, USA (<http://www.esrl.noaa.gov/psd/>) is used in Fig. 12b to validate the model in terms of geopotential height analysis.

3 Influence of the South America orography over regional precipitation

In the following sections, we will firstly describe the influence of the BP and Andes orography in terms of precipitation anomalies. Some regional atmospheric circulation anomalies will also be analyzed.

3.1 Precipitation

Figure 2 shows that removing different orographic structures (Fig. 2a, b) leads to changes more or less pronounced depending on the rainfall structure (Fig. 2c, d), when compared to CTRL (Fig. 1c). The monsoon maximum is still displayed at a similar magnitude in both experiments, but with a more westward expansion in the case of NOANDES (Fig. 2d). However, the SACZ position and magnitude show drastic changes in both removal cases. The coastal SACZ maximum situated in southeastern Brazil in CTRL is clearly decreased in the two experiments, but displaced in opposite direction (Fig. 3). The SACZ is moved southwestward in NOBP (Fig. 2c), but northeastward in NOANDES (Fig. 2d). In NOBP, the displacement is such that the SACZ band structure is almost suppressed and the maximum coastal precipitation reaches the northern portion of

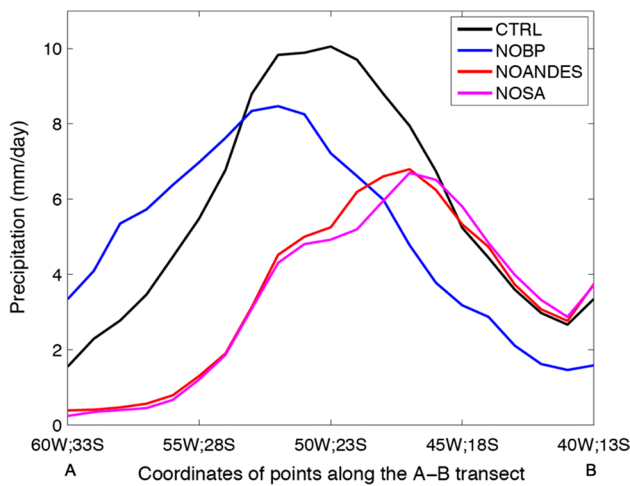


Fig. 3 Precipitation values in mm/day of the A–B section displayed in Fig. 2d, from LMDZ-regional of the CTRL (black line), NOBP (blue line), NOANDES (red line) and NOSA (pink line) experiments

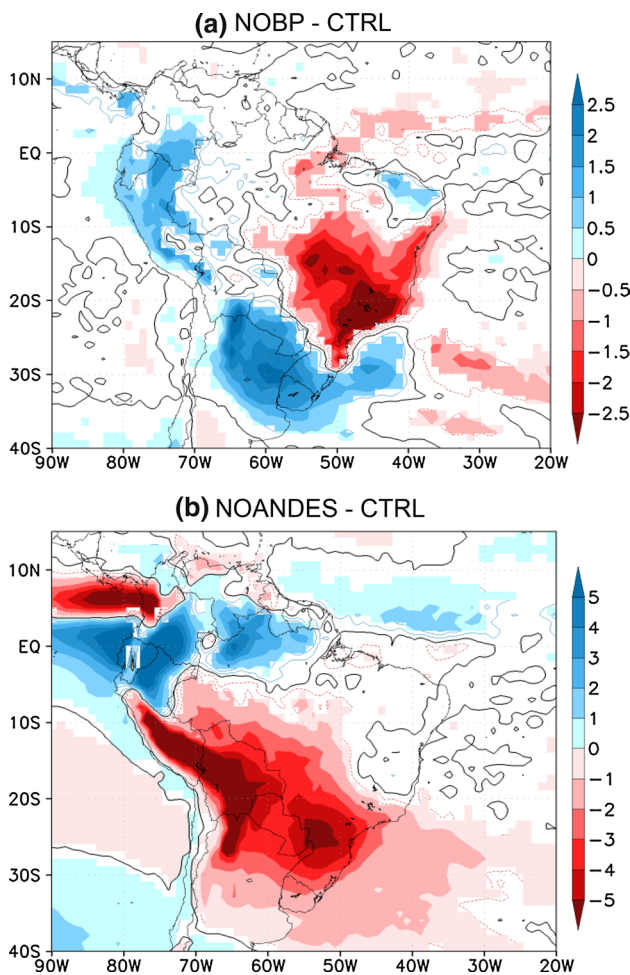


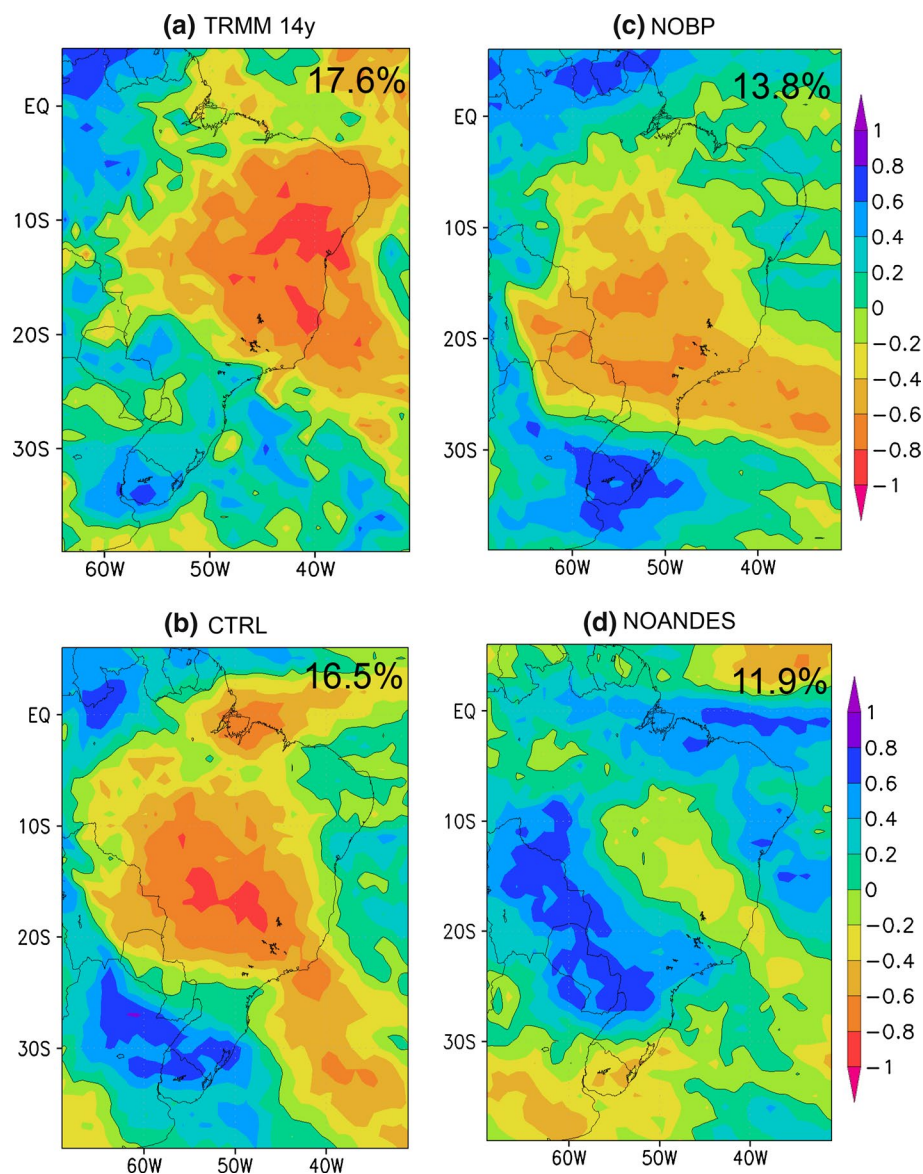
Fig. 4 DJF precipitation differences from LMDZ-regional for **a** NOBP-CTRL, and **b** NOANDES-CTRL. Only the statistically significant values at the 95 % of the Student *t* test are shaded. Values are in mm/day

the SESA region (Fig. 2c). However, the SACZ maximum is displaced twice further in NOANDES than in NOBP (Fig. 3). In addition, when comparing both NOANDES and NOBP with CTRL, it is clear that the suppression of the Andes induces a precipitation decrease of about 40 % in this coastal SACZ maximum zone, while the suppression of the BP is associated with a decrease of about 20 %. These results suggest a stronger control from the Andes to the maximum precipitation of the SACZ in terms of precipitation amount as well as in terms of spatial position of the coastal maximum, while the northwest-southeast band structure of the SACZ seems mainly controlled by the BP.

In SESA, the BP and Andes suppression clearly shows opposite precipitation changes (Fig. 4) associated with two distinctive structure anomalies. When the Andes are removed, a significant decrease is found over a large zone including the southeastern coast of South America from 20 to 40°S, SESA, the southern SACZ and its oceanic part, and all the central-western side of South America (Fig. 4b). On the other hand, the BP suppression produces a significant SESA/SACZ dipole-like anomaly structure (Fig. 4a) with positive anomalies in SESA and negative anomalies in the SACZ region. Figure 3 shows that in the vicinity of point A (see Fig. 2c), situated in SESA, precipitation in NOBP is increased by about twice its value in CTRL, while in NOANDES it is largely decreased, to almost 0. This result suggests that the presence of the Andes is particularly crucial to preserve the actual climatological summer precipitation in the subtropical plains of South America.

As mentioned in Introduction, the leading pattern of the precipitation in eastern South America at a large range of variability is a dipole structure with centers of actions situated in the SACZ region and SESA respectively (e.g., Nogués-Paegle and Mo 1997; Doyle and Barros 2002; Robertson and Mechoso 2000). As shown in Junquas et al. (2012), the evolution of this dipole pattern is a key element to understand the future evolution of precipitation over SESA in greenhouse gases increase scenarios. An EOF analysis is then performed in order to analyze the influence of both the Andes and the BP over the SESA/SACZ dipole-like mode. The EOF analysis is made with the 30 DJF of each experiment, which are taken as 30 individual members. The variation among the 30 members is considered as an internal variability of the experiments. The first EOF of this analysis is displayed in Fig. 5b for the CTRL experiment. For comparison, the EOF analysis of the DJF interannual variability of the 14-DJF TRMM data was performed (Fig. 5a). The structure of the observed DJF leading mode is clearly a dipole between SESA and the SACZ region. The model displays a similar SESA/SACZ dipole-like with the SACZ center situated more southwestward than the dipole displayed by TRMM, the position of the SACZ also being situated more southwestward in the model than in TRMM.

Fig. 5 First mode of EOF analysis performed over **a** the 14 DJF of TRMM 3B43 (1998–2012), and over the 30 members of the **b** CTRL, **c** NOBP, **d** NOANDES experiments. Explained variance is mentioned in each panel



When the BP is removed (Fig. 5c), the dipole is displayed with the two centers of action displaced southwestward, following the displacement of the precipitation maximum associated with the coastal SACZ maximum. This result suggests that the presence of the BP controls the location of the dipole centers, as already argued by Grimm et al. (2007). On the other hand, when the Andes are removed (Fig. 5d), the dipole structure almost disappears from the EOF1, being apparent only in the second EOF mode (not shown). The first EOF displays a tri-pole between northern Argentina and northeastern Brazil, and a North/South dipole in the Atlantic ITCZ. As the ITCZ dipole is not displayed in the CTRL EOF1, it is argued that the first mode of variability of the SACZ in NOANDES is more related to the ITCZ north/south variability than the SESA/SACZ precipitation variability. Then, the presence

of the Andes seems crucial for the SESA/SACZ dipole variability to be the first mode of precipitation variability in eastern South America. As this work only takes into account the internal variability of the atmospheric model, further studies should be performed by performing orography suppression with specific DJF case studies variability analysis instead of a DJF climatology, in order to confirm this result.

The oceanic part of the SACZ is also influenced by the two orographic structures but with smaller magnitudes than its continental counterpart (Fig. 4), the SST being prescribed and unchanged. The oceanic and continental parts of the SACZ are not driven by the same processes. The oceanic SACZ is more influenced by the South Atlantic Anticyclone and transient activity, while the continental SACZ is more affected by the monsoon and the Atlantic

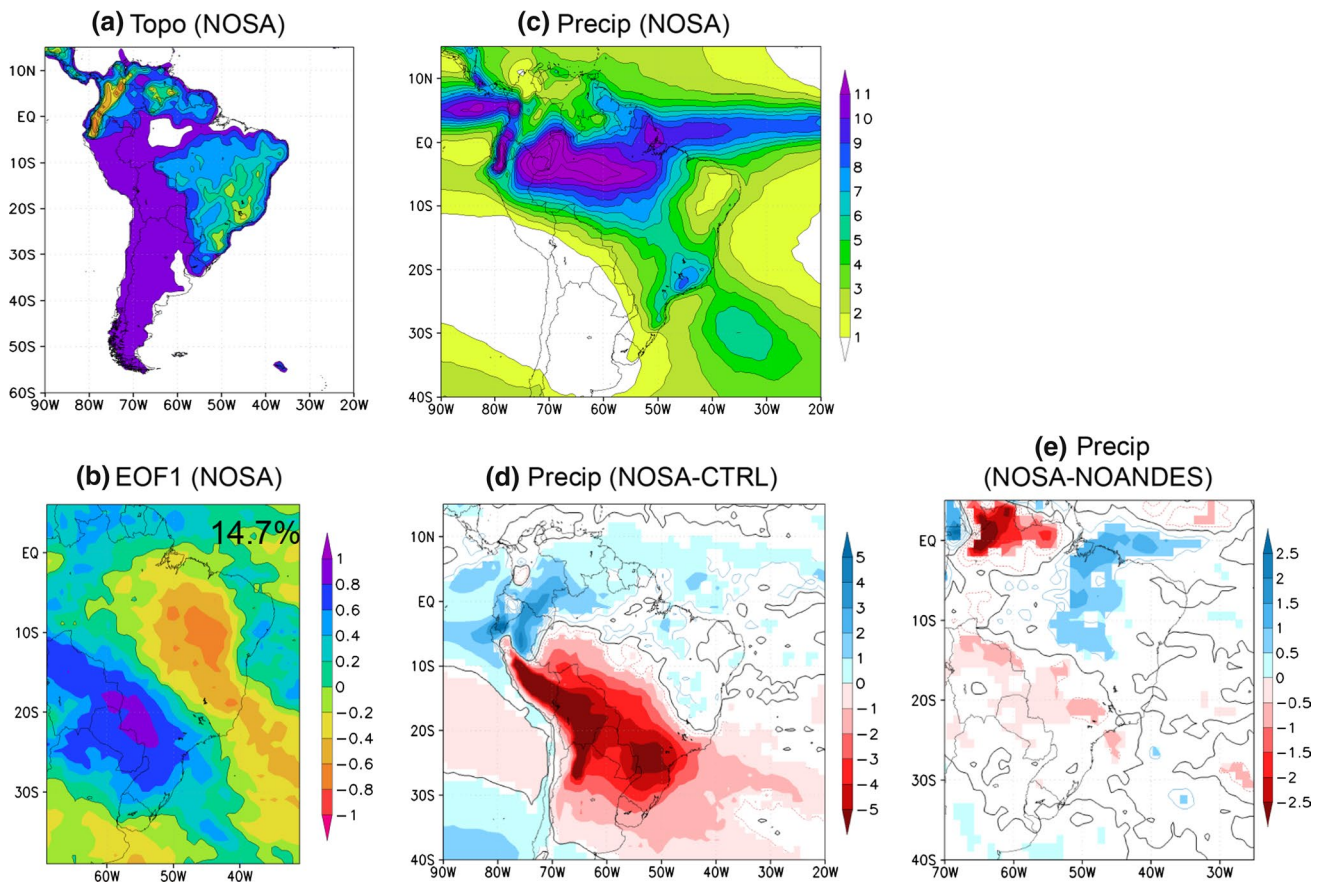


Fig. 6 **a** As in Fig. 1a but for the NOSA experiment, **b** as in Fig. 5b but for NOSA, **c** as in Fig. 1c but for NOSA, **d** as in Fig. 4a but for the difference between NOSA and CTRL, **e** as in Fig. 4a but for the difference between NOSA and NOANDES

ITCZ intensity (e.g. Carvalho et al. 2002, 2004). Precipitation changes in the Pacific and Atlantic ITCZ are found in both experiments. In NOANDES a clear southward displacement of the Pacific ITCZ seems to be associated with the westward expansion of the monsoon (Fig. 4b). Opposite changes are displayed in the Atlantic ITCZ, with a significant increase and northward shift in NOANDES, and a significant decrease and southward shift in NOBP, when compared to CTRL.

Since the Atlantic ITCZ could be directly influenced by the northern orography structure, and particularly the Guiana shield, and in order to explore how much of the Andes influence is associated with its southern and its northern part (including the Guiana shield), an additional experiment was performed, where only the southern Andes, south of 4°S, are removed (see Table 1). Those results are displayed in Fig. 6. The structure of precipitation displayed in NOSA (Fig. 6c) as well as the anomalies induced by the suppression of the southern Andes (Fig. 6d) are close to those found for NOANDES (Fig. 2d for the mean structure, Fig. 4b for the induced anomalies). Then the suppression of the Southern Andes is sufficient to explain the

main features resulting from the suppression of the whole Andes including the shifts in the position and intensity of the SACZ coastal precipitation maximum (Fig. 3). However, the northward displacement of the Atlantic ITCZ in NOANDES (Fig. 4b) is not displayed in NOSA (Fig. 6d, e), suggesting that the northern topography could play a role in establishing the position of the western Atlantic ITCZ. In addition an EOF analysis applied to the NOSA precipitation (Fig. 6b) shows a clear dipole structure between SESA and the SACZ region, but no ITCZ north/south dipole structure. This result suggests an important role of the northern topography over the ITCZ stability. The EOF analysis performed with TRMM and CTRL show that the northern center of the SACZ dipole varies together with the southern part of the Atlantic ITCZ (Fig. 5a, b). It is also the case in NOSA (Fig. 6b). However, in NOANDES the pole centers are of phase opposition (Fig. 5d). The precipitation difference between NOSA and NOANDES (Fig. 6e) shows that the position of the ITCZ in NOANDES is significantly to the north, compared to NOSA. The northward migration of the ITCZ could explain the disconnection between northern SACZ and the southern ITCZ variabilities. In addition, in

NOANDES, the internal ITCZ variability seems increased in comparison with CTRL (Fig. 5). It is then argued that a relative stable ITCZ, in association with the presence of the northern orography, establishes the SESA/SACZ dipole as the first mode of precipitation variability in the region.

3.2 Atmospheric circulation

The precipitation anomalies induced by the BP and the Andes are associated with distinctive atmospheric processes. While NOBP shows a clear anticyclonic circulation anomaly associated with the SESA/SACZ dipole-like precipitation anomaly (Fig. 8a), NOANDES displays a strong weakening of the southward humidity flux over a large part of the continent, associated with the precipitation decrease over the subtropics (Figs. 7c, 8b).

The South Atlantic and Pacific anticyclones are also differently affected by the two experiments. While in NOBP the western part of the South Atlantic Anticyclone seems to penetrate more into the continent (Fig. 7b), the Andes suppression produces a clear penetration of the eastern part of the South Pacific Anticyclone. Such processes could be associated with the opposite displacement of the SACZ (Sect. 3.1). In CTRL, two southward humidity fluxes are found over South America (Fig. 7d). The western flux corresponds to the seasonal mean of the LLJ, and the eastern one is the western branch of the South Atlantic Anticyclone. It is clear that in NOBP the LLJ mean activity at 22°S is intensified and located closer to the eastern slope of the Andes (Fig. 7e), while the eastern branch almost disappears. Between 17 and 20°S, a weak eastern branch is still present to the east of the continent, but much weaker than in CTRL (not shown). South of 20°S, the two structures join together to form one principal southward flux close to the Andes. Those results show that the presence of the BP topography contributes to dissociate the two branches of the southward moisture flux. In NOANDES, the LLJ branch is considerably reduced, and displaced northeastward (Fig. 7f), in opposition with the NOBP experiment. While in CTRL the eastern branch of the SPA is mechanically blocked by the Andes, it penetrates into the continent in the NOANDES experiment, contributing to dry the subtropical region of South America, as also mentioned in Insel et al. (2010). The penetration of the westerly winds from the Pacific Ocean could also increase the ventilation process, as described by Chou and Neelin (2001), contributing to diminish the southward extension of the SACZ.

To sum up, the southwestward displacement of the SACZ in NOBP is associated with the westward displacement of the South Atlantic Anticyclone and a localized anticyclonic circulation anomaly between SESA and the SACZ region. On the other hand, the northeastward displacement of the SACZ in NOANDES is associated with

an eastward displacement of the SPA and a strong weakening of the LLJ mean activity. Therefore, while the effect of the BP over the SESA precipitation is clearly associated with its influence over the regional atmospheric circulation, the Andes influence is mainly related to the humidity transport at the continental scale from the tropics toward the subtropics.

Circulation changes are also found in the northern part of the continent. The NOANDES experiment shows very localized circulation anomalies in this region induced by the removal of both the northern Andes and the Guiana shield. The NOSA experiment displays in average the same atmospheric circulation structure as CTRL in the north of the continent (not shown). The structure of the monsoon maximum is mainly induced by the topography situated to the north of 4°S, playing in particular a role of barrier for the cross-equator monsoon flow (not shown).

In the southern tropics (between 15°S and the equator), Fig. 8a displays a weakening of the southward moisture flux in the northern part of the LLJ region, in association with the BP suppression. Consequently, less moisture is transported southward from the Amazon basin and the moisture flux convergence is increased in the western part of the Amazon basin, where precipitation increases (Fig. 4a). The precipitation increase in the western Amazon in association with an anticyclonic circulation anomaly between the SACZ and SESA regions has also been found in a previous paper through distinct sensitivity experiments, but with the same model configuration (Junquas et al. 2013). It would be interesting to perform DJF case studies of such localized forcing in order to validate and analyze the process.

To summarise, two rainfall structures can be impacted distinctly in South America: the ITCZ and the monsoon in the north, and the SACZ in the south. The BP and South Andes exert their influences through the South Atlantic and South Pacific Anticyclones respectively. Their impacts are mainly on the LLJ and the SACZ, with small effects in the North. On the other hand, the northern topography exerts mainly influences on the ITCZ and the monsoon. However, since the monsoon and the ITCZ variability influences in turn the continental SACZ variability (Carvalho et al. 2002, 2004), the northern topography also affects the SESA/SACZ precipitation dipole variability.

4 Global atmospheric changes

Although the orographic changes simulated in this paper are only located in the South American continent, changes at global scale are expected. This issue is studied in this section, using the results of the NOANDES and NOBP experiments.

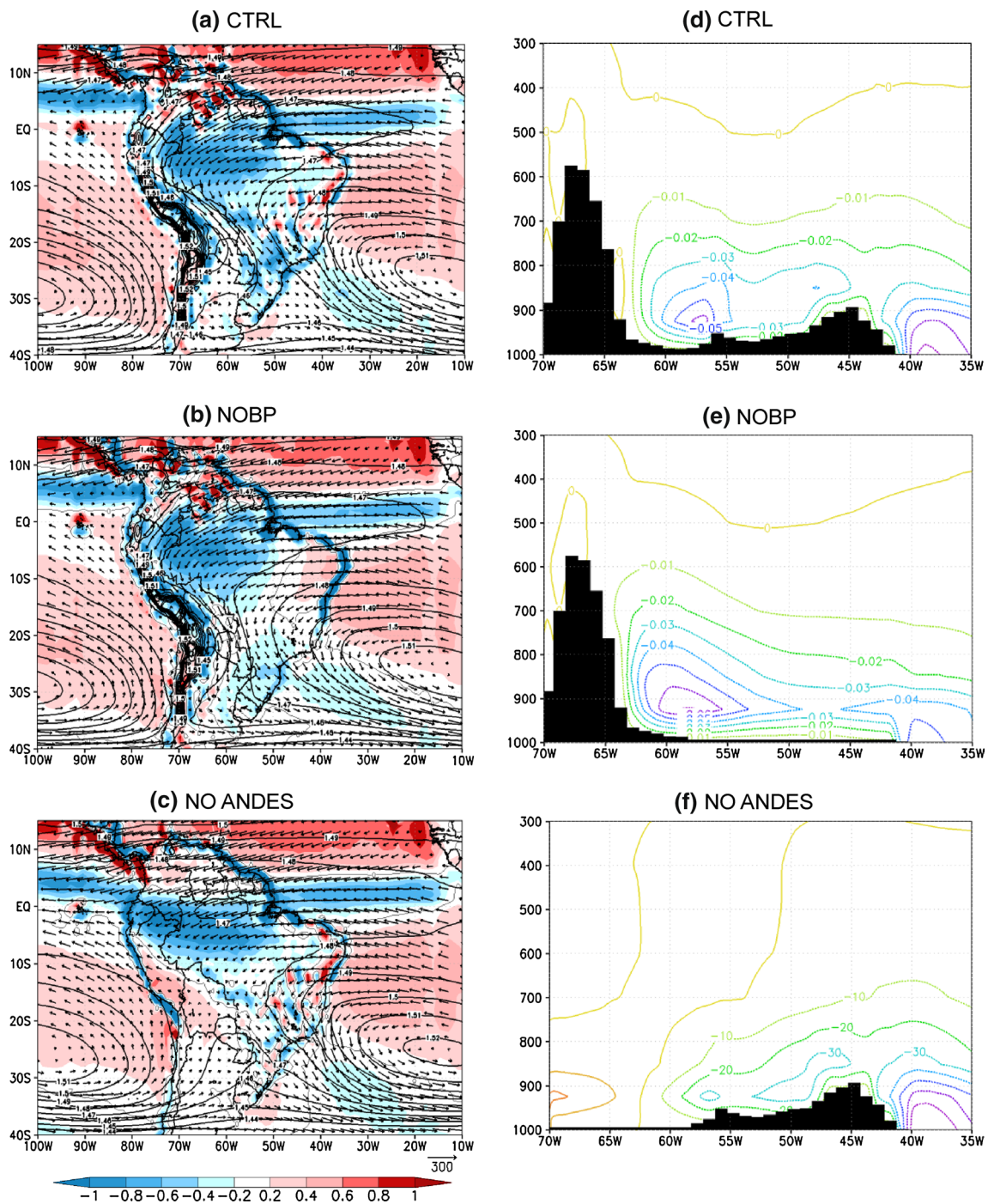


Fig. 7 a–c Vertically-integrated humidity flux between 1000 and 300 hPa (arrows), its divergence (shaded), and the 850-hPa geopotential height (black contours) and d–f vertical section of the meridional humidity flux at 22°S between 70 and 35°W from the LMDZ-

regional, for a, d CTRL, b, e NOBP, c, f NOANDES. For a–c, color scale interval of divergence is $0.2 \text{ kg m}^{-2} \text{ s}^{-1}$. Reference vector of $300 \text{ kg m}^{-1} \text{ s}^{-1}$ is displayed at the lower right corner of c. Contour interval is 10 m. For d–f, contour interval is $10 \text{ m kg m}^{-1} \text{ s}^{-1}$

4.1 Precipitation and low-level atmospheric circulation

The mean precipitation of each experiment is displayed in Fig. 9. The suppression of the Andes clearly induces changes in precipitation patterns, associated with low-level

atmospheric circulation changes (Fig. 9). In the eastern South Pacific, the suppression of the Andes has a mechanical effect over the SPA with its eastern branch penetrating in the western part of the South American continent, as also mentioned in Sect. 3.2 (Fig. 7c). The northern branch of

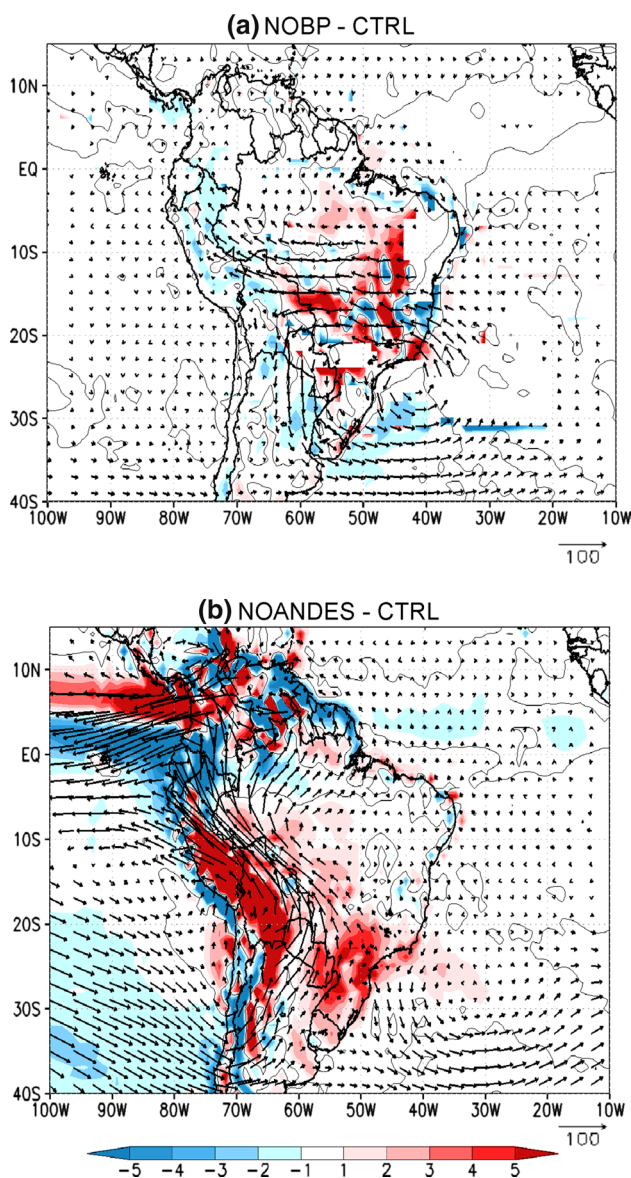


Fig. 8 Difference of the vertically-integrated humidity flux between 1000 and 300 hPa (arrows) and its divergence (shaded) from LMDZ-regional, between **a** NOBP and CTRL, and **b** NOANDES and CTRL. Only the statistically significant values at the 95 % of the Student *t* test are shaded. Color scale interval of divergence is $1 \times 10^{-5} \text{ kg m}^{-2} \text{ s}^{-1}$. Reference vector of $100 \text{ kg m}^{-1} \text{ s}^{-1}$ is displayed at the lower right corner

the SPA migrates northward, and both the SPA and SPCZ take an inclination with a more zonal orientation, compared to CTRL (Fig. 9a). The southern part of the SPCZ is more extended and displaced closer to the coast of South America. The coastal humidity flux associated with the northeastern branch of the SPA is accelerated in the case of NOANDES (Fig. 7c). The westward humidity flux coming from the Amazon region is no longer blocked by the Andes and goes much more to the west, giving abundant

humidity to the tropical eastern Pacific flow, and producing a southward displacement of the eastern Pacific ITCZ (Fig. 10a). These changes are accompanied with a decrease of the north–south expansion of the minimum precipitation region in the eastern South Pacific along the coast of South America (Fig. 9b). This minimum rainfall area is also expanded westward between 10 and 20°S, following the inclination of the SPCZ and the SPA. These results confirm the important role of the trade winds and the humidity flux in the extension of this dry zone, as shown by Takahashi and Battisti (2007a; see Introduction). Precipitation anomalies also show a southeastward displacement of the SPCZ, with negative precipitation anomalies in its western and northern edge, but an increase over its central and eastern part, extending in the South Pacific between 30 and 50°S.

Figure 10b reveals that the BP removal also induces precipitation anomalies at global scale, although with weaker amplitude than for the removal of the Andes. Significant changes are mainly situated over the western equatorial Pacific Ocean and equatorial Indian Ocean. No significant low-level atmospheric circulation anomalies are found in the eastern South Pacific (Fig. 8a). However, the precipitation anomalies induced in NOBP in the western equatorial Pacific region are quite similar to those in NOANDES (Fig. 10a), and also suggest a southeastward displacement of the SPCZ. In the equatorial Indian Ocean, the precipitation anomalies induced by the BP and the Andes removal are opposed. While the Andes suppression is associated with an intensification (weakening) of the eastern (western) part of the Indian Ocean ITCZ (Fig. 10a), the removal of the BP is related to a westward displacement of this pattern, with opposite anomalies (Fig. 10b). Globally, the three subtropical anticyclones (Indian, Pacific and Atlantic) seem displaced northward in both experiments (Fig. 10), and particularly in the NOANDES experiment.

4.2 Large-scale atmospheric teleconnection

Large-scale remote anomalies have been identified in response to the removal of the BP and the Andes topography. A large number of possible teleconnection processes can be directly or indirectly involved. They may be generated by a change in the tropical convection or by a localized atmospheric circulation anomaly. In what follows we describe the large-scale teleconnection anomalies in terms of the Walker circulation, quasi-stationary Rossby waves, stationary equatorial waves, the tropospheric Southern Hemisphere jet-stream, and the Southern annular mode (SAM).

4.2.1 Walker circulation

The DJF Walker circulation in the tropics mainly manifests as a two-wave pattern for the 200-hPa velocity potential,

Fig. 9 DJF Precipitation mean (shaded) and streamlines of the 850-hPa wind (lines) and its divergence, from LMDZ-global, for **a** CTRL, **b** NOBP, **c** NOANDES. Shaded color scale interval is 1 mm/day. Streamlines color scale is $0.1 \times 10^{-5} \text{ kg m}^{-2} \text{ s}^{-1}$

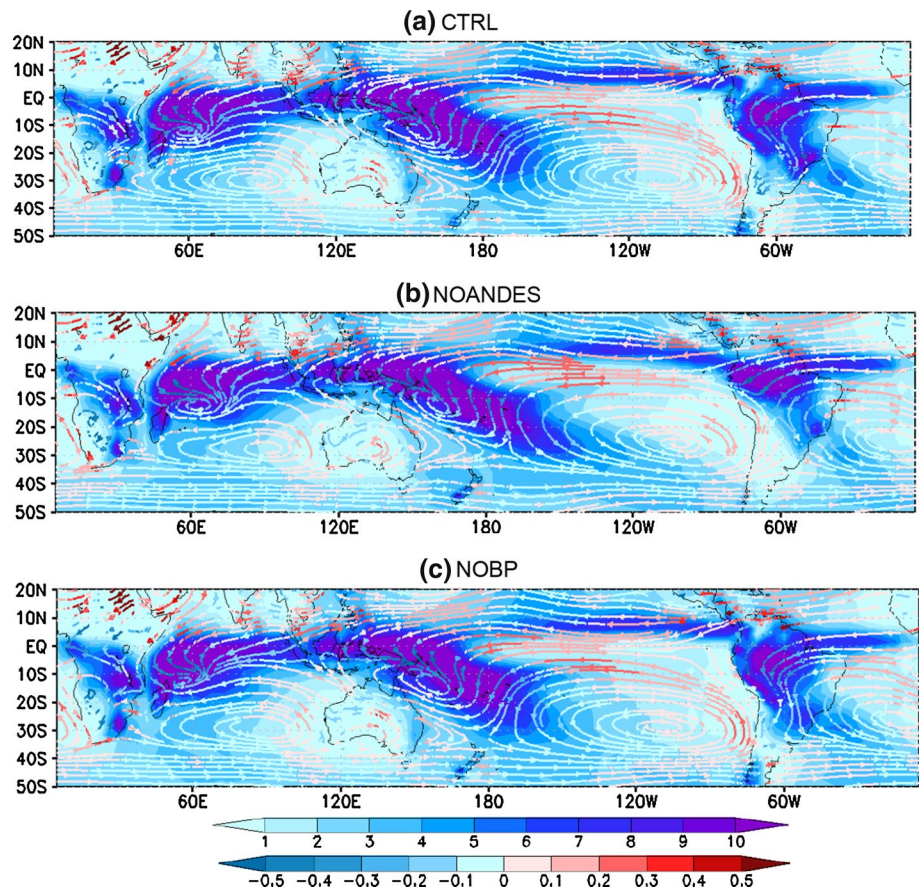
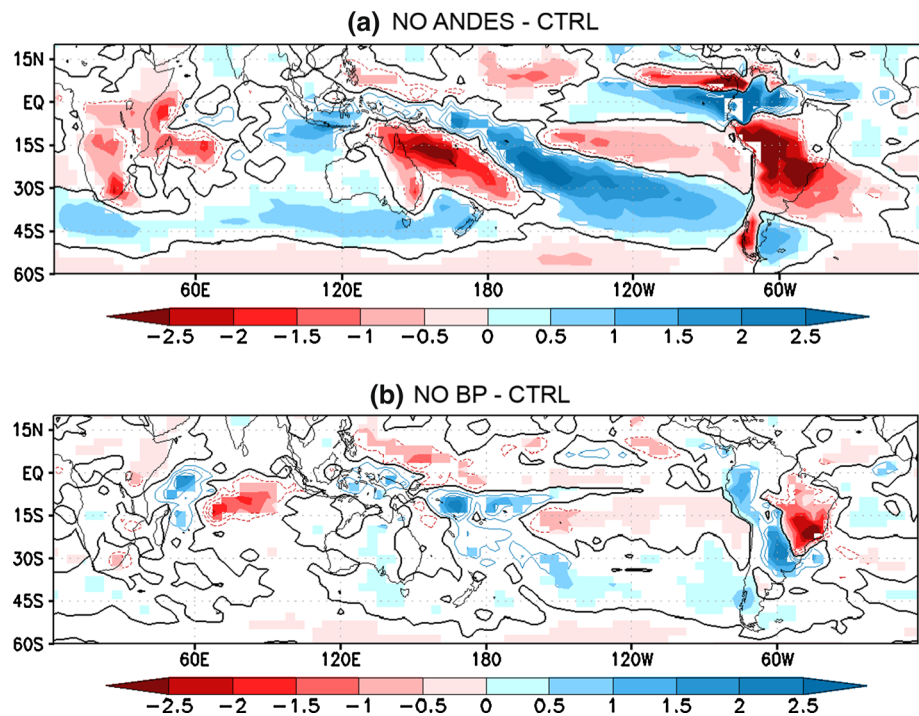


Fig. 10 Difference of the DJF mean precipitation from LMDZ-global between **a** NOANDES and CTRL, **b** NOBP and NOBP. The zero contour is in thick black contour. Only the statistically significant values at the 95 % of the Student *t* test are shaded. Units are mm/day



representing the upward motion centers at the equatorial western Pacific and South America, and the downward motions at the eastern Pacific and eastern equatorial

Atlantic (e.g., Tanaka et al. 2004). Figure 11a shows that the model is able to display similar structures in the CTRL experiment, as well as in NOBP and NOANDES

experiments (not shown). However, if we perform a difference between NOANDES and CTRL (Fig. 11b), we obtain global changes with positive and negative anomalies forming a two-wave structure. The negative anomalies are situated over the eastern Pacific and Indian Ocean, while the positive ones are situated over the western Pacific, and a large area including two centers over South America and the western Indian Ocean. The Indian and Pacific anomalies seem related to the eastward displacement of the Indian ITCZ and the SPCZ respectively. The South American anomaly is associated with the large-scale downward motion produced by the large precipitation anomaly center over the subtropics and central South America, as previously described (Fig. 10a). In the South-eastern Pacific, our results are in agreement with previous studies showing that the suppression of the Andes decreases the large-scale

downward motion in this region, through the suppression of the Andes blocking effect of the westerlies flow (e.g., Rodwell and Hoskins 2001; Takahashi and Battisti 2007a).

The difference between NOBP and CTRL (Fig. 11c) indicates a similar structure as for NOANDES in the equatorial Pacific and South America. However, the equatorial Indian dipole pattern is opposed, as for the precipitation anomalies (Fig. 10b). Globally, the velocity potential anomalies are coherent with the precipitation anomalies found in Fig. 10a, b (for NOANDES and NOBP respectively), showing negative (subsidence) anomalies in regions of precipitation decrease, and positive (ascendance) anomalies in regions of precipitation increase. Such a situation suggests that the weakening of the SACZ produced by the suppression of both orography structures is associated with a re-adjustment of the large-scale vertical motion affecting remote regions such as the western Pacific and Indian Ocean.

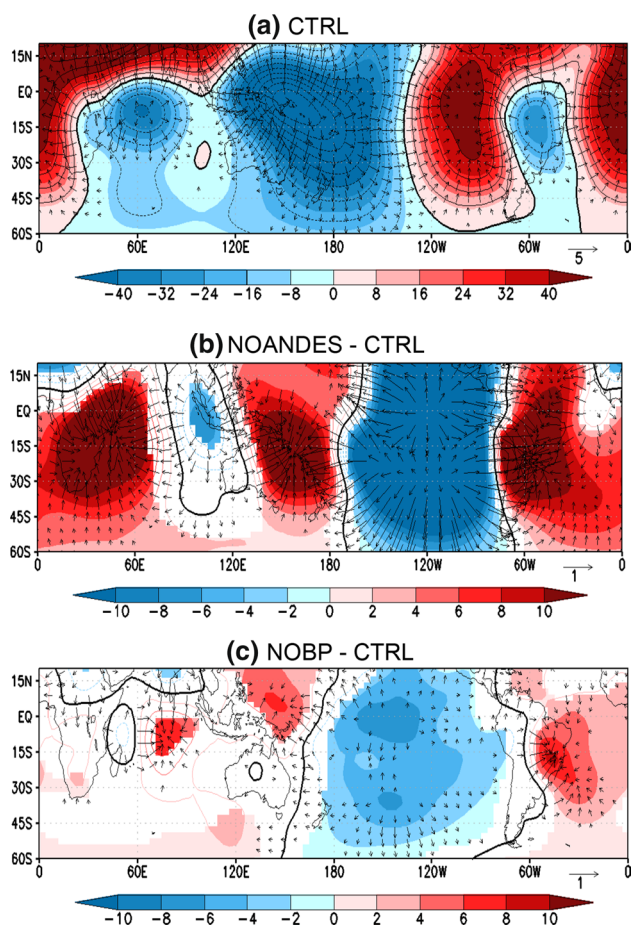


Fig. 11 200-hPa Velocity potential and divergent wind from LMDZ-global for **a** CTRL, and the difference between **b** NOANDES and CTRL, and **c** NOBP and CTRL. Only the statistically significant values at the 95 % of the Student t test are shaded. Color scale and contour interval is **a** $8 \times 10^5 \text{ m}^2 \text{ s}^{-1}$ and **b**, **c** $2 \times 10^5 \text{ m}^2 \text{ s}^{-1}$. In **b**, **c** only the statistically significant values at the 95 % of the Student t test are shaded. Black thick contour indicates the 0 level. Reference vector is displayed at the lower right corner in m s^{-1}

4.2.2 Rossby wave trains

The consequences of both orography changes over the Rossby wave trains in terms of wave sources and energy dispersion are displayed in Fig. 12. The zonal deviation of 500-hPa geopotential height of CTRL, the associated horizontal wave flux activity, and the Rossby wave source term (Vera et al. 2004) are displayed in Fig. 12a. A Rossby wave train-like structure extended along an arch path from the tropical sectors of the Indian and western Pacific Oceans towards South America is evident. As mentioned in the Introduction, this well-known structure, usually called Pacific-South American (PSA) teleconnection pattern, is a key factor to describe how the remote variability, such as that of the tropical convection linked with the SPCZ activity, can influence regional circulation anomalies in South America (e.g., Karoly 1989; Liebmann et al. 1999; Mo 2000; Silva et al. 2009; Grimm et al. 2000). Nevertheless, the development of these quasi-stationary waves can be influenced not only by tropical sources but also by the extratropical circulation dynamics. The model is able to simulate the two main tropical wave sources (i.e. the Indian and western Pacific convection centers) reproduced by NCEP (Fig. 12b). The position of that in the western Pacific is displayed westward in the model, due to a westward bias in the SPCZ location (Junquas et al. 2013). The circulation anomaly centers in NCEP exhibit a wavenumber 1 structure, which is not that evident in the model simulations. In the southeastern Pacific and off southern Chile at 70°S the model over-estimates a negative Rossby center. The activity flux is eastward in both the model and the Reanalysis data, revealing a connection between the South Pacific and South Atlantic Oceans. However this connection is weaker in Reanalysis than in the model. Various studies based on

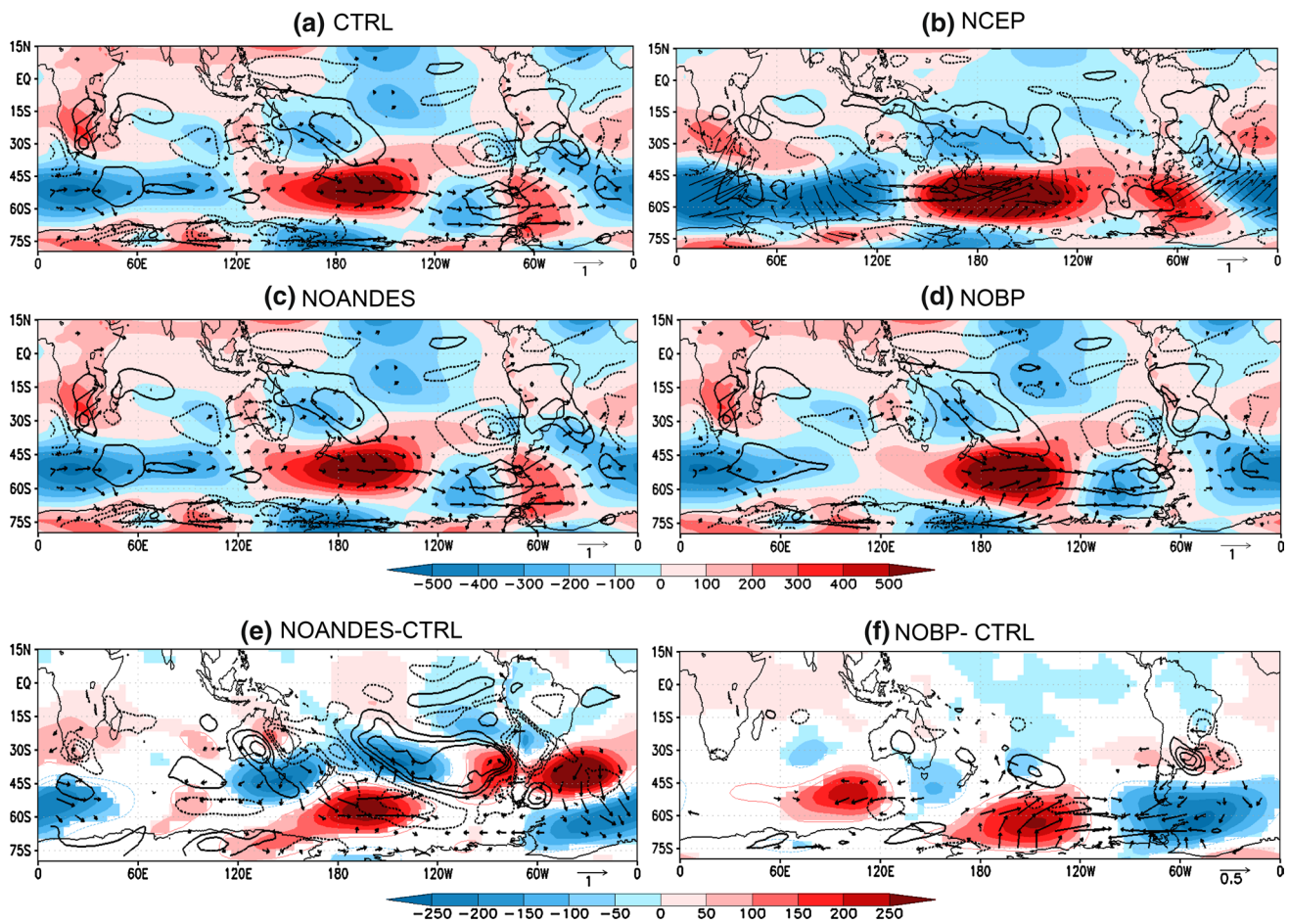


Fig. 12 Zonal deviation of the 500-hPa geopotential height (*shaded*) anomalies from the LMDZ-global, for **a** CTRL, **b** NCEP, **c** NOANDES, **d** NOBP, and the difference **e** between NOANDES and CTRL, **f** between NOBP and CTRL. In **e**, **f**, only the statistically significant values at the 95 % of the Student *t* test are *shaded*. Color scale and colored contour interval is $100 \text{ m}^2 \text{ s}^{-2}$ for the mean fields, and $50 \text{ m}^2 \text{ s}^{-2}$ for the differences. Vectors represent horizon-

tal wave flux activity based on the 500-hPa geopotential height zonal deviation anomalies. Reference vector is displayed at the lower right corner in $10^{-9} \text{ m}^2 \text{ s}^{-3}$. Thick black contours are the 200-hPa Rossby wave source term, with interval of $0.1 \times 10^{10} \text{ s}^{-2}$ ($0.5 \times 10^{10} \text{ s}^{-2}$ for NCEP) and the zero level omitted. The anomalies in **e**, **f** correspond to the difference between **c**, **a**, and between **d**, **a**, respectively, for each field

Reanalysis data found the PSA pattern as the second and third leading mode of the interannual circulation variability in the southern hemisphere, in association with the ENSO events (e.g., Kidson 1999; Mo 2000; Vera et al. 2004). The leading mode of interannual variation in those studies is a different structure, with zonally symmetric anomalies usually associated with fluctuations in the strength of the subtropical jet. The PSA pattern was also described at intra-seasonal and decadal variabilities (e.g., Liebmann et al. 1999; Kidson 1999), and is clearly an important teleconnection mechanism that is part of the time-scale variability of the southern hemisphere climate. However, the relative influence of both the Rossby wave train teleconnection and the subtropical jet fluctuation mechanism in the climatological mean state of the southern hemisphere circulation is unclear. In our results, the climatological DJF mean from

NCEP reanalysis (Fig. 12b) shows more zonally symmetric anomalies related to the subtropical jet fluctuation than in the model (Fig. 12a). The simulations are forced by a DJF climatological SST mean (see Sect. 2.1) that could induce a teleconnection bias relative to the forcing SST mean pattern. Therefore, by displaying a clear Rossby wave train structure in the climatological DJF mean, the model seems to overestimate the influence of the PSA pattern variability in the South Pacific circulation. However, the circulation patterns in the vicinity of South America are very similar. In NOANDES and NOBP (Fig. 12c, d), some differences are discernible in the structure of the wave train as well as in its source centers (Fig. 12d, e) as compared with those in CTRL.

In NOANDES, the Rossby wave source anomalies (Fig. 12d) are well related with rainfall anomalies

(Fig. 10a). They are mainly associated with the SPCZ displacement, and in particular its eastward zonal extension. Strong anomalies are also found in South America and over the eastern South Pacific, in association with the quasi-disappearance of the LLJ and the penetration of the eastern branch of the SPA over the continent. In addition, Fig. 12b shows that the wave-flux activity is increased in the eastern part of the South Pacific, but considerably reduced in its western part. The wave train turns equatorward over the eastern South Pacific instead of western South Atlantic (CTRL, Fig. 12a). It reaches only the southwestern part of South America, and its propagation over SESA and the SACZ region are reduced. The Andes seem to control the trajectory of the equatorward propagation of the Rossby wave train in South America, which affects in turn the role of the teleconnection processes in South America.

In NOBP, the main positive anomaly of Rossby-wave source center is situated in SESA (Fig. 12e) where precipitation increases due to the southwestward displacement of the coastal SACZ maximum (Fig. 4a). As in NOANDES, other anomaly centers are found over the South Pacific, mainly related to the SPCZ displacement. The Rossby-wave activity flux anomalies show a decrease of the equatorward flux over South America (Fig. 12c), but also an increase of northward flux anomalies from polar latitudes (Fig. 12e). In South America, the wave train related anomalies in terms of geopotential height are characterized by a cyclonic anomaly center in the south, and an anticyclonic anomaly center is found over SESA, as already mentioned in Sect. 3.2. If we compare the Rossby wave train teleconnection structures between NOBP (Fig. 12c) and CTRL (Fig. 12a), it is clear that the suppression of the BP reduces the energy dispersion through the wave train from the South Pacific into South America, weakening the teleconnection processes between the western Pacific and the subtropics of South America. So the Andes and the BP orographic structures both play a role in the Rossby wave train teleconnection processes affecting the climate of South America.

The consequences of both orography changes over the Rossby wave trains in terms of wave sources and energy dispersion are displayed in Fig. 12.

4.2.3 Midlatitude jetstream and the Southern annular mode (SAM)

Previous papers showed that subpolar and subtropical jetstreams in the Southern Hemisphere act as waveguides for disturbances emanating from tropical convection centers (e.g., Berbery et al. 1992; Hoskins and Ambrizzi 1993). It can then be argued that the Rossby wave train disturbances previously described could be possibly associated with anomalies of the subtropical Jetstream. Figure 13a shows the 300-hPa zonal mean zonal wind for each experiment.

The zonal wind maximum at 45°S indicates the location of a midlatitude Jetstream, corresponding to the subtropical and subpolar Southern Hemisphere jets merging together during austral summer. In both NOANDES and NOBP it is clear that this midlatitude jetstream is reduced and displaced northward, which could explain the northward displacement of the three Southern Hemisphere anticyclones, found in Fig. 9 (see Sect. 4.1). In NOANDES, the zonal mean flow anomalies show a stronger equatorward displacement of the zonal flow than in NOBP. In addition, Fig. 13b, c show the 500-hPa geopotential height anomalies in a southern polar projection. A dipole is clearly displayed, with positive values over the polar cap and negative values between 45 and 60°S.

Poleward Jetstream shifts have been observed in the last decades (e.g., Marshall 2003; Fu et al. 2006). These shifts have been associated with a trend of the Southern Hemisphere Annular Mode (SAM) towards its positive phase (e.g., Thompson and Solomon 2002). A positive SAM phase is commonly defined as negative geopotential height anomalies over the polar cap, and positive westerly zonal flow anomalies along 60°S (e.g., Thompson et al. 2000, 2005). In addition, Chen and Held (2007) found from both observations and models that the poleward shift of the midlatitude jetstream is associated with an increase of the maximum zonal wind near the tropopause, through an acceleration of the eastward phase speeds of midlatitude eddies. NOBP and NOANDES experiments show anomalies coherent with such mechanisms, although with opposite signs: a decrease of the maximum tropopause zonal wind speed, an equatorward midlatitude jetstream shift, and a negative SAM phase anomaly. In other words, while the mentioned studies concern the recent global climate evolution, we found that the global re-adjustment induced by the presence of a localized orography structure such as the Andes or the BP also induces such changes.

These processes might be mainly explained by the response of the SAM variability to the changes in Rossby wave activity. Ding et al. (2012, 2014) showed that the SAM variability could be significantly influenced by the tropical convection variability through the activity of the Rossby wave train teleconnection. However, various studies described a feedback between the SAM variability and the baroclinic wave activity: the source of the wave follows the north/south movement of the midlatitude jetstream, but on the other hand the propagation of the baroclinic wave activity away from the jet gives momentum fluxes into the jet (e.g. Lorenz and Hartmann 2001; Codron 2005). In both experiments, we found that the equatorward Rossby wave train activity flux are reduced in the South America longitudes (Fig. 13d, e), that possibly explains the decrease of the midlatitude jetstream and the associated changes. However, wave activity flux anomalies are also found in

Fig. 13 **a** Zonal mean zonal wind at 300 hPa for CTRL (black line), NOANDES (red line), NOBP (green line), the difference between NOANDES and CTRL (orange line), the difference between NOBP and CTRL (purple line), from outputs of LMDZ-global. Wind values are in m s^{-1} . **b** 500-hPa geopotential height for the differences NOBP minus CTRL and **c** NOANDES minus CTRL. Only the statistically significant values at the 95 % of the Student *t* test are shaded. Color scale is in $\text{m}^2 \text{s}^{-2}$ and dotted lines are displayed from -90 to -10°S every 10° latitude, and every 60° longitude

other parts of the Southern Hemisphere, which makes difficult the respective identification of responses and forcing mechanisms.

4.2.4 Stationary equatorial waves

It is well known that tropical convection associated with monsoon systems generate distinctive patterns of equatorial quasistationary waves. Figueroa et al. (1995) showed that the latent heat released by the South American monsoon generates an atmospheric circulation pattern very similar to that described by the Gill’s model associated with a combination of Rossby and Kelvin modes (Gill 1980; James 1995). That combination is associated with a rotational circulation component associated with the Bolivian High and the Nordeste Low and a divergent circulation component associated with an upper-level divergence right over the tropical precipitation region and upper-level convergence over the Northeast Brazil and tropical eastern Pacific.

A decrease of the tropical convection in South America is clearly displayed in association with NOANDES (Fig. 11b), and is specifically associated with to the SACZ decrease (Fig. 10a). Consistent with the baroclinic Rossby wave response, this precipitation decrease appears to force the upper-level cyclonic circulation anomaly (Fig. 14) that extends westward above South America, as well as the anticyclonic circulation anomaly at low level (Fig. 8b), as proposed by Rodwell and Hoskins (2001). The associated northeastward displacement of the SPA (Fig. 8b) favors the contraction of the southeast Pacific dry zone (its southern part) and the eastward displacement of the SPCZ (Fig. 9a, b), which could be expected to be even more pronounced if the SST could adjust (Takahashi and Battisti 2007a, b). In addition, Chen et al. (1999) have shown that the South American convection center is part of a global short-wave regime associated with 2–6 wave patterns, also maintained by the African-Indian Ocean convection region. The DJF tropical-subtropical circulation in the SH is largely explained by a combination of this short-wave regime and a long-wave regime associated with the Indian-western Pacific convection system (Chen et al. 1999). Modification

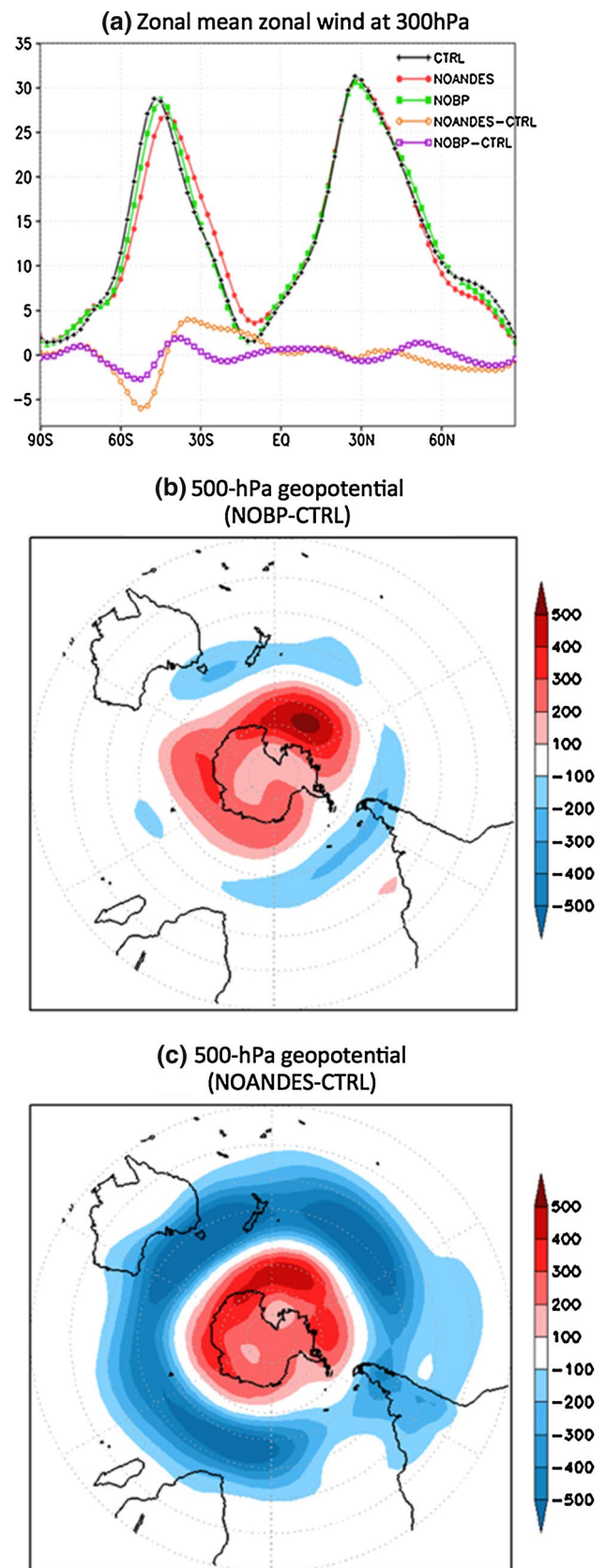
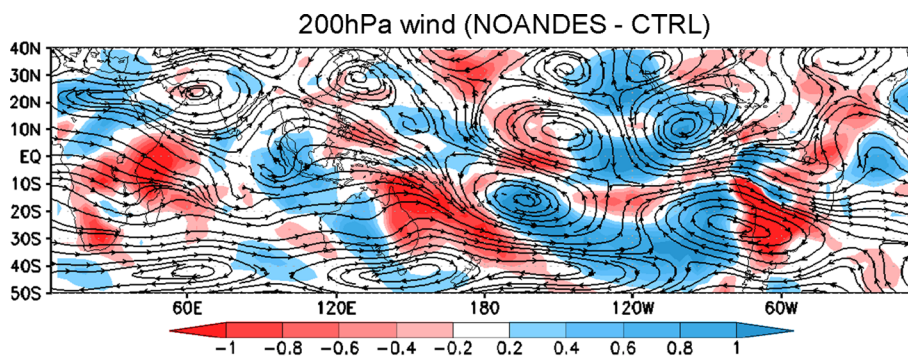


Fig. 14 200 hPa Wind streamlines and its divergence (colors) for the difference between NOANDES and CTRL. Only the statistically significant values at the 95 % of the Student t test are shaded. Color scale is $0.2 \times 10^{-7} \text{ s}^{-1}$, the zero value is omitted



of the South American convection via orographic changes clearly affect these circulations (Figs. 11, 14) and could explain part of the global re-adjustment of the climate system.

5 Summary and discussion

The complex orography of South America provides a basic configuration for the regional climate and constrains the climatological precipitation structures, as well as the monsoon maximum, the SACZ orientation and its coastal maximum position and intensity, or the dipole-like variability between SESA and the SACZ region. These issues are revisited in this paper with the TWN-LMDZ climate model system. We performed sensitivity experiments by removing the three topography structures of South America: the BP, the central and southern Andes (South of 4°S), and the northern South American orography, including the Guiana shield and the northern Andes. For more clarity, we sum up the main changes induced by NOBP and NOANDES experiments in Fig. 15. Locally, the displacement of the SACZ coastal maximum and the Atlantic and Pacific Anticyclones circulation are displayed. The schemes also include some changes in teleconnection processes found in this paper, particularly in terms of Rossby waves, midlatitude jetstream, and SAM anomalies.

Results globally show that the orography control over the precipitation is explained primarily through the mechanical forcing over the regional low-level atmospheric circulation, and particularly over the warm summer monsoon flow into the Amazon region, the low-level jet activity (position and strength) between the Andes and the BP, and the coastal extension of the South Atlantic subtropical high and the South Pacific subtropical high, in particular the western branch of the South Atlantic Anticyclone and the eastern branch of the SPA. The orography of South America also induces global-scale consequences by re-adjustment of the general circulation. Changes of precipitation were found in remote areas, as for the SPCZ or the Indian ITCZ, associated with large-scale atmospheric circulation

changes, including anomalies in the Walker circulation vertical motions, a decrease and an equatorward displacement of the midlatitude jet, a negative SAM phase anomaly, Rossby wave train teleconnection anomalies, and stationary equatorial waves anomalies.

5.1 Brazilian Plateau

Previous studies have found that the presence of the BP is characterized by a regional control of both the regional precipitation and low-level circulation, as mentioned in Introduction (Grimm et al. 2007; Kodama et al. 2012). Our results confirm their main results, as for example the southwestward displacement of the SACZ and its weakening, and an increase of the precipitation in SESA due to the suppression of the mountains. As these previous works were based on particular case studies, we show here that those orographic control features also concern the climatological summertime mean. In addition, our results also revealed organized high-level atmospheric circulation anomalies in response to the removal of the BP.

The BP removal also produces global teleconnection processes. The decrease of the SACZ intensity due to the suppression of the plateau induces a weakening of the upward motion of the zonal overturning circulation situated in South America. On the other hand, the propagation of the Rossby wave train from the western tropical Pacific is locally affected by the local atmospheric circulation anomalies. The equatorward propagation of the wave train over South America is reduced, decreasing its interaction with the local subtropical climate. In addition, an equatorward displacement of the southern midlatitude jetstream is found, together with a weak equatorward shift of the Indian, South Pacific and South Atlantic anticyclones, and associated precipitation changes in the Indian and Pacific oceans. A negative SAM phase anomaly is also displayed in association with the decrease of the maximum zonal wind near the tropopause between 45 and 60°S . Such processes are coherent with previous studies that explain how the SAM mode, the midlatitude Jetstream and the baroclinic wave activity are connected (see Sect. 4.2).

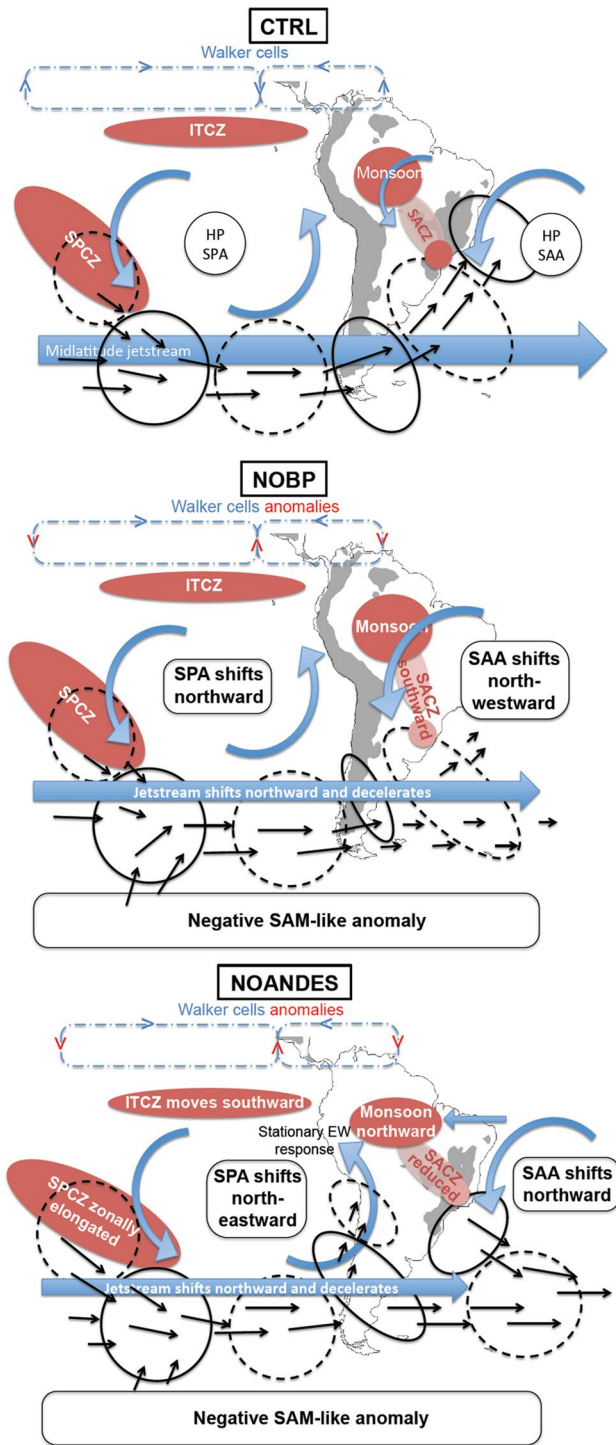


Fig. 15 Schematic diagrams of the main results. Red ellipses correspond to rainfall patterns, and blue arrows concern atmospheric circulation structures. Black arrows and ellipses represent Rossby wave activity flux and zonal mean geopotential anomalies respectively. The changes in Walker cells atmospheric circulation is represented in dashed blue lines. EW means equatorial waves. The role of the northern topography is not represented here

The influence of the BP orography over the South America regional climate is not only explained by direct regional processes, but also by global feedbacks and teleconnection processes. Since the differentiation of the direct regional effect and the regional-global-regional control of the orography over the climate in south-eastern South America have not been performed here, it is not clear yet how much the global teleconnection processes contribute to the regional effect.

5.2 Andes

The suppression of the Andes also induces both regional and global changes in terms of precipitation and atmospheric circulation. In particular, our results confirm that the Andes are crucial for the LLJ activity, as already shown in previous studies (e.g., Gandu and Geisler 1991; Campetella and Vera 2002; Insel et al. 2010; Saurral et al. 2014; see Introduction). Our results also suggest that there is a strong control of the Andes over the position and intensity of the SACZ coastal maximum. Figueroa et al. (1995) already pointed out the importance of the Andes in the position of the SACZ. However, in their results, the presence of the Andes induced a displacement of the coastal SACZ in the opposite direction of the displacement found in our results (Fig. 3). This difference could be explained by the fact that they used a relatively low-resolution model (2.5° grid), and that they did not consider the influence of the BP in their no-Andes sensitivity test. More recently, Insel et al. (2010) used a 60-km resolution model to perform sensitivity tests with no Andes, and considering the BP topography. They found a weak precipitation decrease in the coastal SACZ but no significant changes in its position. They argued that the SACZ is mainly related with the heat release of the Amazon basin, and the convergence between the humidity flow coming from the Amazon with the western branch of the South Atlantic Anticyclone. However, according to the key role of the LLJ activity in the humidity transport from the tropics toward the subtropics of South America (e.g., Berbery and Barros 2002), our results suggest that the Andes also controls the intensity of the southwestern part of the SACZ, by controlling its humidity supply from the LLJ. In this study, we showed in particular that the climatological position of the SACZ is associated with the mechanical effect of the Andes over the LLJ activity, and that without this effect, the SACZ maximum would be located in a more northeastward position. In addition, in agreement with Chou and Neelin (2001), our results also show that the presence of the Andes, via its control over the humidity advection from the Pacific westerlies, could also influence the southern extension of the SACZ in the South American continent.

At large scale, the suppression of the Andes also induces atmospheric circulation and precipitation anomalies in remote areas of the globe, being the consequences of various teleconnection mechanisms. As for the no-BP experiment, the suppression of the Andes and the associated weakening of the SACZ also induce a weakening of the convective system in South America. However, the suppression of the mechanical effect of the Andes (including the Guiana shield) induces an increase and northward displacement of the equatorial Amazonia monsoon maximum. A global equatorward displacement, in terms of southern hemisphere midlatitude jetstream, and subtropical anticyclones, is found in both no-BP and no-Andes experiments. But it is stronger in the latter. A negative phase anomaly of SAM is also found stronger in the no-Andes experiment than in the no-BP one. The wave-activity flux associated with the Rossby wave train is also modified, and shows in particular a decrease and eastward displacement of its equatorward propagation wave in South America. This enhances the influence on the western coast of South America, but strongly reduces the impact in the eastern coast.

In this work, we also analyzed the distinct role of the southern and northern topography of South America, including the northern Andes and the Guiana shield. Results show that the southern Andes are responsible of the major changes induced by the whole Andes in terms of precipitation and low-level atmospheric circulation in southern and eastern South America. However, the northern topography has a key role over the stability of the Atlantic ITCZ. When the northern topography is reduced, the first mode of inter-member variability in the region is more related to the north/south dipole pattern associated with displacements of the ITCZ than to the dipole-like pattern between SESA and the SACZ region.

5.3 Discussion

In this paper we identified a large list of mechanisms that interact to determine how orography acts on the precipitation patterns in South America, and particularly in SESA. We investigated four main global teleconnection processes associated with changes in the South America orography: (1) the global Walker circulation, (2) Rossby wave trains, (3) the SAM and the midlatitude jet position and strength, and (4) a Gill's model-like response corresponding to stationary equatorial waves to the west of the Amazon. The Walker circulation anomaly seems to reflect a global re-adjustment of the main large-scale ascendance and subsidence zones. For this process as well as for the stationary equatorial waves anomaly, the changes in the Amazon convection is the key regional triggering mechanism activating this global adjustment, as both the Andes and the BP control the Amazon convection through their impacts on

the SACZ. We argue that this global re-adjustment mainly explains how changes in the South American orography induce changes in remote convection zones. The Rossby wave trains and SAM anomalies seem in turn associated with the equatorial convection anomalies situated in South America, western Pacific and Indian Ocean. Therefore, these processes are also part of the global re-adjustment, and the respective responses and forcing remote mechanisms are not identified yet.

Previous studies showed that the effect of the Andes over the eastern Pacific is mainly driven by changes in the dry zone expansion, as mentioned in Introduction (Xu et al. 2004; Takahashi and Battisti 2007a, b). However, our results suggest a strong control of the SPCZ and the SPA position. We found in agreement with these studies that the suppression of the Andes induces a weaker subsidence, the suppression of the blocking of the warm monsoon easterlies, and the reduction of the northward extension of the dry zone. But we also found an increase of the westward expansion of the dry zone, in association with the westerlies strengthening and the northward displacement of the SPA. Some differences between their experiments and ours could explain this difference. First, we only used an atmospheric model, without ocean coupling as in Takahashi and Battisti (2007a, b), therefore drastically limiting the ocean-atmosphere feedback. In addition, our results do not take into account a clear double-ITCZ feedback as in Xu et al. (2004), since this feature is very weak in our CTRL experiment. In their no-Andes simulation, they did not find such a strong northward SPA displacement as in our results, including the penetration of dry westerly wind in the south-west of the continent, but Insel et al. (2010) found such a penetration, associated with the quasi-disappearance of the LLJ activity. Nevertheless, additional simulations should be performed with coupling our atmospheric LMDZ-TWN system with an oceanic system, in order to combine the effect of the SPCZ and SPA changes with the air-sea feedback processes of the dry zone.

It is interesting to note that both the BP and the Andes show influences over the South Atlantic and Pacific Anticyclones. While the BP mainly controls the position of the western branch of the South Atlantic Anticyclone, the Andes control the position and intensity of the SPA. Those results are in agreement with Rodwell and Hoskins (2001), who showed that the subtropical anticyclone circulations are related with the monsoon activity. Our results show that the presence of the BP and the Andes contributes to increase the SACZ, a key component of the South American monsoon (e.g., Kodama 1992). It is clear in our results that the SACZ increase related to the presence of the Andes induces an increase of both the SPA and the large-scale subsidence west of the Andes, confirming the large-scale control of the monsoon activity over its western side,

characterizing an equatorial waves response to the monsoon heating. On the other hand the presence of the BP is associated with a strengthening of the northern part of the LLJ activity, as well as the western branch of the South Atlantic Anticyclone. Rodwell and Hoskins (2001) showed that the poleward jet of the western branch of the Anticyclone is a Kelvin wave response to the monsoon heating over the continent to the West. However, while the presence of the Andes clearly increases the LLJ activity, the presence of the BP seems to separate the poleward flow into two branches, one being known as the LLJ itself, and the other one over the eastern part of the continent, being part of the humidity flux convergence characterizing the coastal SACZ maximum.

Mountains influence over large-scale atmospheric circulation and precipitation can be explained by mechanical effects (e.g., Hahn and Manabe 1975) and thermal effects (e.g., Wu et al. 2012), both being connected through dynamical processes (e.g., Duan and Wu 2005). While these two effects were largely studied for the Tibetan Plateau and Himalayas mountains, as in the previous cited studies, few studies analyzed them separately for the South America topography. Kodama et al. (2012) showed that the precipitation increase induced by the development of the SACZ over the BP maximum topography was explained by a local cyclonic circulation due to the SACZ heating and maintained by the presence of the orography. Our results also suggest such a thermal circulation feature. In addition it is shown that the mechanical control of the BP over the LLJ orientation maintains part of its humidity flow toward the southwestern part of the SACZ, contributing to increase the precipitation in its coastal part. Our results suggest that the coastal SACZ maximum is controlled by both thermal and mechanical effects.

As mentioned in Sect. 2.1, the SACZ region suffers a too-strong precipitation bias in our control experiment. The presence of the BP orography enhances this bias. While the southwestward displacement of the SACZ was found as the main consequence of the removed BP, a weakening of the maximum precipitation was also found. However, this maximum, even displaced and weakened, still exists in the no-BP simulation, showing that other processes contribute to this model bias. In fact, the precipitation maximum in the no-BP case is obtained through a convergence of the LLJ and the western branch of the South Atlantic Anticyclone. Therefore in addition to orographic processes, thermodynamic processes are also responsible of this model bias. Further sensitivity experiments to thermodynamic processes are needed for a better understanding of this issue.

Previous studies removing orography used different spin-up methodologies depending on the experiment duration and the orography height. Insel et al. (2010) performed

a 10-years experiment without the Andes, of which results based on the last 5-years of simulation were considered. However, in studies where the BP was reduced, Kodama et al. (2012) and Grimm et al. (2007) performed respectively 10- and 7-days of spin-up in order to perform a 1-month experiment. Rodwell and Hoskins (2001) analyzed in more details this issue, and conclude that in the boundary layer, 5 days are sufficient to the system to absorb the hydrostatic adjustments, and until 25 days for much of the atmosphere. Our methodology includes gradual step periods plus the period of 1 month of spin-up, which although on the short side, appears sufficient for the system to spin up (including the establishment of planetary waves, and mass and energy balance), considering that the initial shock is very localized and not very strong. However, further investigations should be pursued in order to identify the adequate spin-up methodology when performing such orographic-changes experiments.

As documented in Junquas et al. (2013; their Fig. 3), our model shows biases, including some regional and global precipitation biases mentioned in Sect. 2.1, that need to be better understood. Therefore our results are to be considered with caution. The physical processes described in this study are proper to our model and to our simulations, and the use of other models would be necessary to confirm them and improve their realism. Therefore, future investigations should be pursued. In particular, as previously mentioned, an adequate coupling between the atmosphere and the ocean would improve the realism of some of the teleconnection anomalies identified, as for instance changes in the South Pacific wave trains. A higher resolution outside the “two-way interaction” zone (South America) could also help to better represent teleconnection mechanisms.

Acknowledgments Comments and suggestions provided by three anonymous reviewers were very helpful in improving this paper. This research was supported by the European Commission’s Seventh Framework Programme (FP7/2007–2013) under Grant Agreement No 212492 (CLARIS LPB. A Europe-South America Network for Climate Change Assessment and Impact Studies in La Plata Basin), ECOS-MINCYT (project No A12U02 DIAGAC), CNRS/LEFE Program, and CONICET PIP 112-200801-00399. The first author C.J. was supported by a Ph.D grant from the Ecole Polytechnique, and post-doc grants from the Institute of Research for the Development (IRD), the French National Center for Scientific Research (CNRS), and the Ecole Polytechnique. We especially thank François Lott, Frédéric Hourdin and our other colleagues from the LMD (Laboratoire de Météorologie Dynamique) for the productive discussions about the experiments.

References

- Berbery E, Barros V (2002) The hydrologic cycle of the la plata basin in South America. *J Hydrometeorol* 3(6):630–645

- Berberly EH, Nogués-Paegle J, Horel JD (1992) Wavelike southern hemisphere extratropical teleconnections. *J Atmos Sci* 49(2):155–177
- Braconnot P, Hourdin F, Bony S, Dufresne JL, Grandpeix JY, Marti O (2007) Impact of different convective cloud schemes on the simulation of the tropical seasonal cycle in a coupled ocean–atmosphere model. *Clim Dyn* 29(5):501–520
- Bretherton CS (1993) Understanding Albrecht’s model of tradecumulus cloud fields. *J Atmos Sci* 50:2264–2283
- Campetella CM, Vera CS (2002) The influence of the Andes Mountains on the South American low-level flow. *Geophys Res Lett* 29(17):1826. doi:10.1029/2002GL015451
- Carvalho LM, Jones C, Liebmann B (2002) Extreme precipitation events in southeastern South America and large-scale convective patterns in the South Atlantic convergence zone. *J Clim* 15(17):2377–2394
- Carvalho LM, Jones C, Liebmann B (2004) The South Atlantic convergence zone: intensity, form, persistence, and relationships with intraseasonal to interannual activity and extreme rainfall. *J Clim* 17(1):88–108
- Carvalho LM, Jones C, Posadas AN, Quiroz R, Bookhagen B, Liebmann B (2012) Precipitation characteristics of the South American monsoon system derived from multiple datasets. *J Clim* 25(13):4600–4620
- Chen G, Held IM (2007) Phase speed spectra and the recent poleward shift of Southern Hemisphere surface westerlies. *Geophys Res Lett* 34(21). doi:10.1029/2007GL031200
- Chen T, Weng S, Schubert S (1999) Maintenance of austral summertime upper-tropospheric circulation over tropical south America: the bolivian high-nordeste low system. *J Atmos Sci* 56:2081–2100
- Chen W, Jiang Z, Li L, Yiou P (2011) Simulation of regional climate change under the IPCC A2 scenario in southeast China. *Clim Dyn* 36:491–507
- Chou C, Neelin JD (2001) Mechanisms limiting the southward extent of the South American summer monsoon. *Geophys Res Lett* 28(12):2433–2436
- Codron F (2005) Relation between annular modes and the mean state: Southern Hemisphere summer. *J Clim* 18:320–330
- Codron F, Sadourny R (2002) Saturation limiters for water vapour advection schemes: impact on orographic precipitation. *Tellus A* 54:338–349
- Davis N, Bowden J, Semazzi F, Xie L, Öno B (2009) Customization of RegCM3 regional climate model for eastern Africa and a tropical Indian Ocean domain. *J Clim* 22(13):3595–3616
- Ding Q, Steig EJ, Battisti DS, Wallace JM (2012) Influence of the Tropics on the Southern Annular Mode. *J Clim* 25(18):6330–6348
- Ding H, Greatbatch RJ, Gollan G (2014) Tropical influence independent of ENSO on the austral summer Southern Annular Mode. *Geophys Res Lett* 41:3643–3648
- Doyle M, Barros V (2002) Midsummer low-level circulation and precipitation in subtropical South America and related sea surface temperature anomalies in the South Atlantic. *J Clim* 15:3394–3410
- Duan AM, Wu GX (2005) Role of the Tibetan Plateau thermal forcing in the summer climate patterns over subtropical Asia. *Clim Dyn* 24(7–8):793–807
- Emanuel KA (1991) A scheme for representing cumulus convection in large-scale models. *J Atmos Sci* 48:2313–2335
- Figueroa S, Satyamurty P, Da Silva Dias PL (1995) Simulations of the summer circulation over the south american region with an eta coordinate model. *J Atmos Sci* 52(10):1573–1584
- Fu Q, Johanson CM, Wallace JM, Reichler T (2006) Enhanced mid-latitude tropospheric warming in satellite measurements. *Science* 312:1179
- Gandu AW, Geisler JE (1991) A primitive equations model study of the effect of topography on the summer circulation over tropical South America. *J Atmos Sci* 48:1822–1836
- Garreaud RD, Rutllant J, Quintana J, Carrasco J, Minnis P (2001) CIMAR-5: a snapshot of the lower troposphere over the subtropical Southeast Pacific. *Bull Am Meteorol Soc* 82:2193–2208
- Gates WL (1992) AMIP: the atmospheric model intercomparison project. *Bull Am Meteorol Soc* 73:1962–1970
- Gill A (1980) Some simple solutions for heat-induced tropical circulation. *Q J R Meteorol Soc* 106(449):447–462
- Grimm A, Barros V, Doyle M (2000) Climate variability in southern south america associated with el niño and la niña events. *J Clim* 13:35–58
- Grimm A, Pal J, Giorgi F (2007) Connection between spring conditions and peak summer monsoon rainfall in South America: role of soil moisture, surface temperature, and topography in eastern brazil. *J Clim* 20(24):5929–5945
- Hahn DG, Manabe S (1975) The role of mountains in the south Asian monsoon circulation. *J Atmos Sci* 32:1515–1541
- Hoskins BJ, Ambrizzi T (1993) Rossby wave propagation on a realistic longitudinally varying flow. *J Atmos Sci* 50(12):1661–1671
- Hourdin F, Musat I, Bony S, Braconnot P, Codron F, Dufresne J, Fairhead L, Filiberti M, Friedlingstein P, Grandpeix J (2006) The lmdz4 general circulation model: climate performance and sensitivity to parametrized physics with emphasis on tropical convection. *Clim Dyn* 27(7):787–813
- Huffman GJ, Adler RF, Bolvin DT, Gu G, Nelkin EJ, Bowman KP, Hong Y, Stocker EF, Wolff DB (2007) The TRMM Multisatellite Precipitation Analysis (TMPA): quasi-global, multiyear, combined-sensor precipitation estimates at fine scales. *J Hydrometeorol* 8:38–55. doi:10.1175/JHM560.1
- Huffman GJ, Bolvin DT, Adler RF (2011) GPCP version 2.2 combined precipitation data set. WDC-A, NCDC, Asheville, NC. Data set accessed at <http://www.ncdc.noaa.gov/oa/wmo/wdcamet-ncdc.html>
- Insel N, Poulsen CJ, Ehlers TA (2010) Influence of the andes mountains on South American moisture transport, convection, and precipitation. *Clim Dyn* 35:1477–1492
- James I N (1995) Introduction to circulating atmospheres. Cambridge University Press, Cambridge
- Junquas C, Vera C, Li L, Le Treut H (2012) Summer precipitation variability over southeastern South America in a global warming scenario. *Clim Dyn* 38:1867–1883
- Junquas C, Vera CS, Li L, Le Treut H (2013) Impact of projected SST changes on summer rainfall in southeastern South America. *Clim Dyn* 40:1569–1589
- Kalnay E, Kanamitsu M, Kistler R, Collins W, Deaven D, Gandin L, Joseph D (1996) The NCEP/NCAR 40-year reanalysis project. *Bull Am Meteorol Soc* 77(3):437–471
- Karoly D (1989) Southern hemisphere circulation features associated with el niño southern oscillation events. *J Clim* 2:1239–1252
- Kidson JW (1999) Principal modes of Southern Hemisphere low-frequency variability obtained from NCEP-NCAR reanalyses. *J Clim* 12(9):2808–2830
- Kodama Y (1992) Large-scale common features of subtropical precipitation zones (the baiu frontal zone, the spcz, and the sacz). I: characteristics of subtropical frontal zones. *J Meteorol Soc Jpn* 70:813–836
- Kodama YM, Sagawa T, Ishida S, Yoshikane T (2012) Roles of the Brazilian Plateau in the formation of the SACZ. *J Clim* 25:1745–1758
- Kummerow C, Simpson J, Thiele O, Barnes W, Chang ATC, Stocker E, Nakamura K (2000) The status of the tropical rainfall measuring mission (TRMM) after two years in orbit. *J Appl Meteorol* 39:1965–1982
- Li Z (1999) Ensemble atmospheric GCM simulation of climate inter-annual variability from 1979 to 1994. *J Clim* 12:986–1001

- Liebmann B, Kiladis GN, Marengo J, Ambrizzi T, Glick JD (1999) Submonthly convective variability over South America and the South Atlantic convergence zone. *J Clim* 12(7):1877–1891
- Lorenz DJ, Hartmann DL (2001) Eddy-zonal flow feedback in the Southern Hemisphere. *J Atmos Sci* 58:3312–3327
- Lorenz P, Jacob D (2005) Influence of regional scale information on the global circulation: a two-way nesting climate simulation. *Geophys Res Lett* 32:L18706. doi:[10.1029/2005GL023351](https://doi.org/10.1029/2005GL023351)
- Marshall GJ (2003) Trends in the southern annular mode from observations and reanalyses. *J Clim* 16:4134–4143
- Marti O et al (2005) The new IPSL climate system model: IPSL-CM4. Note du Pôle de Modélisation No. 26. Institut Pierre Simon Laplace des Sciences de l'Environnement Global, Paris. <http://dods.ipsl.jussieu.fr/omamce/IPSLCM4/DocIPSLCM4/FILES/DocIPSLCM4.pdf>
- Mesinger F, Janjic ZI, Nickovic S, Gavrilov D, Deaven DG (1988) The step-mountain coordinate: model description and performance for cases of Alpine lee cyclogenesis and for a case of an Appalachian redevelopment. *Mon Weather Rev* 116:1493–1518
- Mitchell TP, Wallace JM (1992) The annual cycle in equatorial convection and sea surface temperature. *J Clim* 5:1140–1156
- Mo K (2000) Relationships between low-frequency variability in the southern hemisphere and sea surface temperature anomalies. *J Clim* 13:3599–3610
- NOAA National Geophysical Data Center (2001) 2-Minute gridded global relief data (ETOPO2), World Data Cent for Mar Geol and Geophys, Boulder, Colo. <http://www.ngdc.noaa.gov/mgg/fliers/01magg04.html>
- Nogués-Paegle J, Mo K (1997) Alternating wet and dry conditions over south america during summer. *Mon Weather Rev* 125:279–291
- Pesquero JF, Chou SC, Nobre CA, Marengo JA (2010) Climate downscaling over South America for 1961–1970 using the Eta Model. *Theor Appl Climatol* 99(1–2):75–93
- Robertson A, Mechoso C (2000) Interannual and interdecadal variability of the South Atlantic convergence zone. *Mon Weather Rev* 128:2947–2957
- Rodwell M, Hoskins B (2001) Subtropical anticyclones and summer monsoons. *J Clim* 14:3192–3211
- Rozante JR, Moreira DS, de Goncalves LGG, Vila DA (2010) Combining TRMM and surface observations of precipitation: technique and validation over South America. *Weather Forecast* 25(3):885–894
- Saurral RI, Camilloni IA, Ambrizzi T (2014) Links between topography, moisture fluxes pathways and precipitation over South America. *Clim Dyn*. doi:[10.1007/s00382-014-2309-z](https://doi.org/10.1007/s00382-014-2309-z)
- Silva G, Ambrizzi T, Marengo J (2009) Observational evidences on the modulation of the south american low level jet east of the andes according the enso variability. *Ann Geophys* 27:645–657. **(Copernicus)**
- Simmons AJ, Burridge DM (1981) An energy and angular-momentum conserving vertical finite-difference scheme and hybrid vertical coordinates. *Mon Weather Rev* 109(4):758–766
- Takahashi K, Battisti DS (2007a) Processes controlling the mean tropical Pacific precipitation pattern. Part I: the Andes and the eastern Pacific ITCZ. *J Clim* 20:3434–3451
- Takahashi K, Battisti DS (2007b) Processes controlling the mean tropical Pacific precipitation pattern. Part II: the SPCZ and the southeast Pacific dry zone. *J Clim* 20(23):5696–5706
- Tanaka H, Ishizaki N, Kitoh A (2004) Trend and interannual variability of walker, monsoon and hadley circulations defined by velocity potential in the upper troposphere. *Tellus A* 56:250–269
- Thompson DWJ, Solomon S (2002) Interpretation of recent Southern Hemisphere climate change. *Science* 296:895–899
- Thompson DW, Wallace JM, Hegerl GC (2000) Annular modes in the extratropical circulation. Part II: trends. *J Clim* 13:1018–1036
- Thompson DWJ, Baldwin MP, Solomon S (2005) Stratosphere-troposphere coupling in the Southern Hemisphere. *J Atmos Sci* 62:708–715
- Vera C, Silvestri G, Barros V, Carril A (2004) Differences in el nino response over the southern hemisphere. *J Clim* 17:1741–1753
- Vera C, Baez J, Douglas M, Emmanuel CB, Marengo J, Meitin J, Nicolini M, Nogue-Paegle J, Paegle J, Penalba O, Salio P, Saulo C, Silva-Dias PL, Zipser E (2006) The South American lowlevel jet experiment. *Bull Am Meteorol Soc* 87:63–77
- Wu G, Liu Y, He B, Bao Q, Duan A, Jin FF (2012) Thermal controls on the Asian summer monsoon. *Sci Rep* 2. doi:[10.1038/srep00404](https://doi.org/10.1038/srep00404)
- Wyant MC, Bretherton CS, Rand HA, Stevens DE (1997) Numerical simulations and a conceptual model of the subtropical marine stratocumulus to trade cumulus transition. *J Atmos Sci* 54:168–192
- Xie P, Arkin P (1997) Global precipitation : a 17-year monthly analysis based on gauge observations, satellite estimates, and numerical model outputs. *Bull Am Meteorol Soc* 78:2539–2558
- Xu H, Wang Y, Xie SP (2004) Effects of the Andes on Eastern Pacific climate: a Regional Atmospheric Model Study. *J Clim* 17(3):589–602
- Yuter SE, Serra Y, Houze RA Jr (2000) The 1997 Pan American climate studies tropical eastern Pacific process study. Part II: stratocumulus region. *Bull Am Meteorol Soc* 81:483–490
- Zhu Z (1997) Precipitation and water vapor transport simulated by a hybrid σ - θ Coordinate GCM. *J Clim* 10:988–1003